A Theoretical Description of Pattern Formation in Thin Solution Layers

Theoretische Beschreibung von Strukturbildung in dünnen Lösungsschichten

als Masterarbeit vorgelegt von
Walter Tewes

Dezember 2013

Westfälische Wilhelms-Universität Münster

Contents

1. Introduction and Motivation

Generally speaking, the topic of the present work is the theoretical description of *thin films* of a *complex fluid*. From the point of view of a theoretical description, the term *thin* does not refer to an absolute height of the film but rather to the ratio of the height to a typical horizontal length scale [KT07]. The variety of liquid films which can be considered as *thin* according to this notation is extremely large, ranging from lava flows, with a height larger than ten meters, to films of a height on the molecular length scale. Reviews of the dynamics and statics of thin films can be found, e.g., in [CM09, ODB97]. However, in the context of technical applications and related experiments, authors often refer to the absolute height of the films as *thin*. There, the main interest is the behavior of liquid films of heights of a few hundred nanometers deposited on solids. Homogeneous coatings of solids by thin liquid films are important for optical applications and are also employed as protective layers [ODB97]. In other cases, e.g., depending on the thickness of the film and the interaction energies between film and underlying solid, thin films eventually break up into more or less regular structures which can be of interest for applications in semiconductor technologies [CWS$^+$02]. Early experiments of this *self-assembly* mechanism in the case of thin polymer films are presented in [Rei92].
These applications motivate the description of thin films on a solid, with a free surface given by the liquid-gas interface. Following common nomenclature, the solid will be subsequently referred to as the *substrate*. The theoretical description of simple liquids, i.e., liquids consisting of a single component, for this geometry is quite advanced. The basic equations are reasonably well understood and of Cahn-Hilliard type as we will see in chapter 4.
In contrast, thin films of binary fluids, exhibiting phase separation and local concentration dependence are still not understood to a large extent. For recent publications related to this topic, see [NT10, TTL13]. Especially the description of solutions, featuring a volatile solvent, is of great interest for the description of deposition processes from thin films. The structured deposition of technically relevant molecules at the contact line of a thin film moving on a substrate has been experimentally investigated in the past decade [Thi14]. By contact line, we refer to the region where the liquid-gas interface meets the solid-liquid interface. The controlled deposition can be obtained, e.g., through the evaporation of a droplet of solution from a restricted geometry as reported in [LG05, HXX$^+$05], but most commonly, controlled deposition is achieved through the use of the so-called *dip-coating* technique. In this intriguingly simple technique, the substrate is pulled from a bath containing the solution and the deposition takes place at the contact line of the *meniscus*, where the solvent evaporation is strongest. A sketch of the experimental set-up is shown in figure 1.1. Two different types of molecules

can be deposited in dip-coating processes, namely surface-active and non surface-active molecules. Surface active molecules are amphiphilic, i.e., consisting of a hydrophilic and a hydrophobic part and are therefore adsorbed at the surface of the solution, forming a so-called *Langmuir-Blodgett* film. A theory concerned with the description of pattern formation during the transfer of such films on a substrate can be found in [KGFC10, LKG$^+$12]. For the case of surface active molecules, which are adsorbed at the surface, the liquid subphase can be treated as a one-component fluid, with a surface layer dependent surface tension.
However, in the past decade various dip-coating experiments were performed using solutions containing non surface-active molecules, which are deposited when the solvent evaporates. Structures found are in general stripe patterns as, e.g., in [GFS07] for the case of colloidal suspensions. A short overview is given in [LKG$^+$12, FAT12].

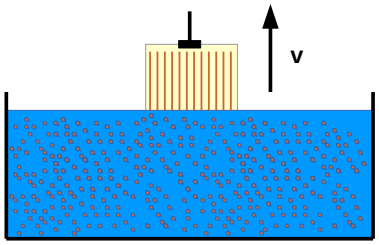

Figure 1.1.: Sketch of the experimental set-up in dip-coating experiments. The substrate is pulled out of a bath filled with a solution with a constant velocity v which is in most cases the main experimental control parameter.

Recently, experiments were performed at the University of Münster, where more complex structures of dendritic type are formed during the deposition of molecules of the organic semiconductor *DTBDT-C9* on silicon wafers [LGS$^+$10] (see figure 1.2 for optical images of the deposition structures and the structural formula of the solute molecules). In these experiments, the main control parameter is the transfer velocity v, i.e., the velocity at which the substrate is pulled out of the bath containing the solution. The velocity determines the morphology of the deposits, as well as the number of layers of which the deposits consist. Bilayer and multilayer deposits exhibit a crystal ordering, whereas the monolayer deposits are reported to be amorphous. Therefore, it seems probable that the dynamical deposition process at the contact line plays a crucial role even for structures as complex as described above.
As stated before, the description of the dynamical formation of such structures from solutions of non surface-active molecules is rather involved. As a first step, one needs to develop thin film equations for solutions, which are valid for dense solutions and evaporating solvents. The formulation and investigation of such equations is addressed in the present thesis.

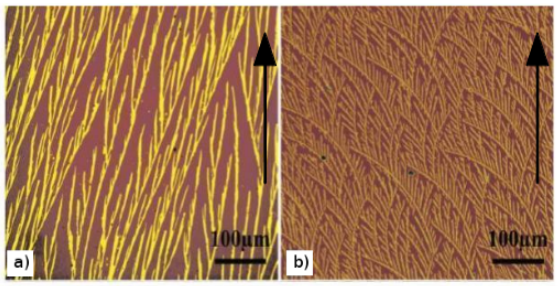

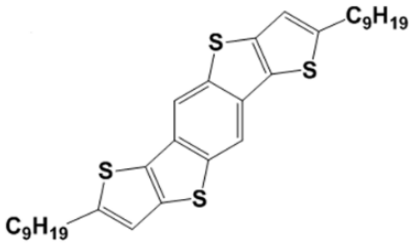

Figure 1.2.: Left: Optical images of (a) multilayer and (b) bilayer deposits of DTBDT on a silicone substrate as reported in [LGS$^+$10]. The pulling direction is indicated by the arrows. Right: Structural formula of DTBDT-C9.

The thesis is organized as follows: Subsequent to the introductory chapter, in the second chapter, the well known advection-diffusion equations for binary fluids will be discussed in details. Using a long-wave expansion, the corresponding equations in the thin film limit will be derived. These resulting equations are coupled, highly nonlinear, partial differential equations for the local height $h(\mathrm{x}, t)$ and the local, height averaged concentration $\phi(\mathrm{x}, t)$ of the solution layer which are only valid for dilute solutions.
In chapter 3, we introduce a gradient formulation of the simple diffusion equation and formulate the Cahn-Hilliard equation as a generalization of this equation. Following [Thi11], it is then shown that the basic equations derived in the previous chapter can also be written in terms of a gradient formulation. In the framework of the gradient formulation, we present an extension of the basic equations through an alteration of the free energy functional and propose a derivation for one part of the resulting equations.
Chapter 4 starts with a discussion of the thin film equations for simple liquids, which are contained as a special case in our equations for solutions. The full extended equations as derived in chapter 3 are then supplemented by an evaporation term. In addition, we perform a linear stability analysis of the full system of equations and discuss some numerical results on the dynamics exhibited by the equations.
While the dynamics shown in the previous chapter take place on a substrate at rest, in chapter 5 we investigate the dynamics on a moving substrate, namely using boundary conditions that mimic the transfer process which occurs in dip-coating experiments. Here, it is shown that periodic structures, i.e., stripes and patterns of hexagonal type, are formed at the meniscus due to evaporation-induced phase decomposition.
The thesis ends with a summary as well as a discussion of the results and an outlook on possibilities and tasks for future work.

2. Derivation of the Basic Equations

2.1. Advection-Diffusion Equations for Solutions

The basic equations for fluids are the Navier-Stokes equation (2.1) for the velocity $\mathbf{u}(\mathbf{x},t)$ and the continuity equation (2.2) for the density $\rho(\mathbf{x},t)$, $\mathbf{x}\in\mathbb{R}^3$ of the fluid [LLW91]:

$$\rho(\partial_t\mathbf{u}+\mathbf{u}\cdot\boldsymbol{\nabla}\mathbf{u}) = -\boldsymbol{\nabla}p+\eta\Delta\mathbf{u}+\left(\xi+\frac{\eta}{3}\right)\boldsymbol{\nabla}(\boldsymbol{\nabla}\cdot\mathbf{u}), \tag{2.1}$$

$$\partial_t\rho+\boldsymbol{\nabla}\cdot(\rho\mathbf{u}) = 0. \tag{2.2}$$

Here, the *Lamé-parameters* of viscosity ξ and η are assumed to be independent of $(\mathbf{x},t)$. Note that the last summand in equation (2.1) is non-zero only for compressible fluids. Following [LLW91], we now wish to extend these equations to a system of equations for two-component fluids, i.e., binary mixtures. These equations can then be applied to solutions of small solute concentration, where the effect of concentration on the Navier-Stokes equation enters only through the dependence of the Lamé-parameters on the concentration. Although the equations will be subject to massive simplifications in the framework of the *lubrication approximation*, in this section they will be presented in their full extend.

The relevant new order parameter for the case of mixtures and solutions is the concentration $c(\mathbf{x},t)$ of one component. The concentration can be defined as a *per mass-*, a *per parts-* or a *per volume* concentration. The relations between the different definitions are in general nonlinear for particles of different size and different mass per mole. In this section, we define $c := c_m$ as a per mass concentration. Later on, we will assume identical particles in mass and size and use the definition of a per volume concentration. To prevent confusions, a few words should be spend on the correspondence of the different definitions with the average density ρ.

Let us consider a small volume element $dV = dV_\mathrm{A}+dV_\mathrm{B}$ containing a small mass element of the fluid $dm = dm_\mathrm{A}+dm_\mathrm{B}$, where $dV_\mathrm{A,B}$ are the volumes occupied by molecules of component A or B, respectively and $dm_\mathrm{A,B}$ are the corresponding masses. We can now define the per mass concentration c_m and the per volume concentration c_V as

$$c_V = \frac{dV_\mathrm{A}}{dV_\mathrm{A}+dV_\mathrm{B}}; \qquad c_m := \frac{dm_\mathrm{A}}{dm_\mathrm{A}+dm_\mathrm{B}} = \frac{\rho_\mathrm{A}dV_\mathrm{A}}{\rho_\mathrm{A}dV_\mathrm{A}+\rho_\mathrm{B}dV_\mathrm{B}} = \frac{\rho_\mathrm{A}c_\mathrm{V}}{\rho}. \tag{2.3}$$

Here, the mass densities $\rho_\mathrm{A,B}$ are the constant densities of the pure substances A,B, whereas the average density of the fluid ρ is defined via $\rho_\mathrm{A}dV_\mathrm{A}+\rho_\mathrm{B}dV_\mathrm{B} := \rho dV$.

The explicit dependence of the average density ρ (which is the density now appearing in the Navier-Stokes equation) on the per mass concentration reads:

$$\rho = \frac{\rho_{\mathrm{A}}\rho_{\mathrm{B}}}{\rho_{\mathrm{B}}c_m + (1-c_m)\rho_{\mathrm{A}}}. \tag{2.4}$$

The overall mass flux of the fluid is given by

$$\mathbf{J}_{\mathrm{A+B}} = \rho\mathbf{u} = c\rho\mathbf{u} + (1-c)\rho\mathbf{u}. \tag{2.5}$$

The velocity $\mathbf{u}$ can be interpreted as a center of mass velocity of the binary fluid.
Let us now consider the spatio-temporal evolution of the mass density ρc of one component, e.g., in the case of a solution, the mass density of the solute. As the mass of the solute is conserved, the corresponding density obeys a local conservation law of the form:

$$\partial_t(\rho c) = -\boldsymbol{\nabla}(\rho c\ \mathbf{u} + \mathbf{J_c}), \tag{2.6}$$

where $\mathbf{J}_{\mathrm{A}} = \rho c\ \mathbf{u}$ is the flux of mass due to advection and $\mathbf{J}_c$ corresponds to the flux due to *diffusion*. Note that through equation (2.5) the diffusive fluxes for the different components are related by $\mathbf{J}_c = -\mathbf{J}_{1-c}$. Using equation (2.2), we obtain the advection-diffusion equation for the concentration of the solute:

$$\rho(\partial_t c + \mathbf{u}\cdot\boldsymbol{\nabla}c) = -\boldsymbol{\nabla}\cdot\mathbf{J}_c. \tag{2.7}$$

The evolution of the overall flow field $\mathbf{u}$ is given by a modified Navier-Stokes equation, where the Lamé-parameters are now in general concentration-dependent and thus spatio-temporally non-constant:

$$\rho(\partial_t\mathbf{u} + \mathbf{u}\cdot\boldsymbol{\nabla}\mathbf{u}) = -\boldsymbol{\nabla}p + \boldsymbol{\nabla}\cdot\boldsymbol{\gamma}. \tag{2.8}$$

Here, $\boldsymbol{\gamma}$ is the viscous stress tensor and in the most general case γ_{ij} reads

$$\gamma_{ij} = \left(\eta(c)\left(\partial_{x_j}\partial u_i + \partial_{x_i}\partial u_j - \frac{2}{3}\delta_{ij}\partial_{x_l}u_l\right)\right) + \delta_{ij}\left(\xi(c)\partial_{x_l}u_l\right). \tag{2.9}$$

We use the notation $\boldsymbol{\nabla}\cdot\boldsymbol{\gamma} := \partial_{x_i}\gamma_{ij}$ and $i,j \in \{1,2,3\}$. Notice that several terms may be omitted in later derivations when assuming approximate incompressibility. In general, for $\rho_A \neq \rho_B$, the average density ρ can not be considered as a constant due to the relation (2.4). To close the system of equations for mixtures and solutions, one finally needs information about the diffusive flux in equation (2.7). In general, the diffusive flux results from temperature gradients, concentration gradients and pressure gradients. For the sake of simplicity, we confine ourselves to the discussion of concentration dependence and refer the reader to [LLW91] for a more detailed discussion of all effects in the framework of thermodynamics. In this case one obtains:

$$\mathbf{J}_c = -\rho D\ \boldsymbol{\nabla}c. \tag{2.10}$$

Here, we call $D = D(c)$ the *diffusion coefficient*, which may be concentration dependent. The suitable concentration dependence for solutions can be formulated indirectly through the concentration dependence of the viscosity and by the well known *Einstein relation*:

$$D(c) = \frac{k_B T}{6\pi a \eta(c)}. \tag{2.11}$$

The relation can be easily derived by considering the thermodynamic equilibrium of a solution in a conservative external force field, as it was done in [Ein06]. In relation (2.11), a is a molecular length of a solute molecule, $\eta(c)$ the viscosity of the fluid, k_B is the Boltzmann constant and T is the temperature. A concentration dependence of the viscosity will be discussed in Chapter 4.

2.2. Lubrication Approximation of the Advection-Diffusion Equations

In this work, we are interested in the dynamics of very thin films of solution, i.e., in systems with largely separated horizontal and vertical length scales. It is quite obvious that in this case approximations through rescaling of the basic equations suggest themselves. For this purpose, we will introduce a vertical length scale h_0 and a horizontal length scale l_0 and use their ratio $\epsilon := \frac{h_0}{l_0}$ as a parameter of smallness. This approximation technique is widely used for thin films and is referred to as *lubrication approximation* or *long-wave expansion*. A review of the treadment of liquids in the thin film limit can be found in [ODB97].
The derivations shown here follow the ideas presented in [WCM03], where the derivation has been performed for equations for soluble but surface active solutes. In [WCM03] thermal effects are also included, which are omitted here in order to obtain a simplified model.
In the framework of the lubrication approximation, partial differential equations for the local height $h(\mathbf{x}, t)$, as well as for the height-averaged local concentration $\phi(\mathbf{x})$ of the thin film of solution, will be derived. Here, $\mathbf{x} = (x, y)$ are the horizontal coordinates (see also figure 2.1). We adopt the notation

$$\mathbf{a^{(3)}} := (a_x, a_y, a_z); \quad \mathbf{a} := (a_x, a_y); \quad \boldsymbol{\nabla}^{(3)} := (\partial_x, \partial_y, \partial_z); \quad \boldsymbol{\nabla} := (\partial_x, \partial_y). \tag{2.12}$$

The following properties of the system in question are assumed:

(a) The vertical extension of the system is much smaller than the horizontal extension.

(b) The diffusion in the vertical direction leads to fast averaging of the concentration in the vertical direction.

(c) The concentration is small throughout the system.

The most important tool for the derivation of simplified equations by using the properties (a)-(c) is the rescaling of the respective equations. We will now introduce the general scaling by length and time scales (h_0, l_0 and t_0 respectively), further scaling will be introduced ad hoc when needed in the derivations. We define (see figure 2.1 for the choice of the coordinate system):

$$z = h_0\tilde{z};\quad \mathbf{x} = l_0\tilde{\mathbf{x}};\quad t = t_0\tilde{t};\quad \mathbf{u} = \frac{l_0}{t_0}\tilde{\mathbf{u}} =: u_0\tilde{\mathbf{u}};\quad u_z = \frac{h_0}{t_0}\tilde{u_z} = \epsilon u_0\tilde{u_z}. \tag{2.13}$$

For the derivatives, we obtain accordingly:

$$\partial_t = \frac{1}{t_0}\partial_{\tilde{t}}\quad \boldsymbol{\nabla} = \frac{\epsilon}{h_0}\tilde{\boldsymbol{\nabla}}\quad \partial_z = \frac{1}{h_0}\partial_z. \tag{2.14}$$

As already mentioned above, the parameter ϵ can be treated as a parameter of smallness to account for assumption (a).

2.2.1. Evolution of the Height Profile

We start out by deriving an equation for the height profile $h(\mathbf{x}, t)$ dependent on the vertically averaged velocity field $\overline{\mathbf{u}} := \frac{1}{h}\int_0^h \mathbf{u}\left(\mathbf{x^{(3)}}\right)\, dz$. An expression for $\overline{\mathbf{u}}$ will be obtained from the Navier-Stokes equation later on. Using assumption (c), we consider ρ to be approximately independent of $(\mathbf{x^{(3)}}, t)$, which is valid for small concentrations c or $\rho_A \approx \rho_B$ in equation (2.4). In this case equation (2.2) reduces to the so-called incompressibility equation:

$$\partial_z u_z = -\partial_x u_x - \partial_y u_y. \tag{2.15}$$

Using the *no-penetration* boundary condition at $z = 0$ ($u_z(z = 0) = 0$), we obtain

$$u_z(\mathbf{x}, h(\mathbf{x}, t), t) = -\int_0^{h(\mathbf{x},t)} \boldsymbol{\nabla}\mathbf{u}\, dz. \tag{2.16}$$

The velocity of the fluid at the surface is $\mathbf{u}^{(3)}(\mathbf{x}, h(\mathbf{x}, t), t)$. We can now introduce a different velocity $\mathbf{u_s^{(3)}}(\mathbf{x}, h(\mathbf{x}, t), t)$ which complies with the identity

$$\frac{d}{dt}h = \partial_t h + \mathbf{u_s}\cdot\boldsymbol{\nabla}h = u_{s,z}. \tag{2.17}$$

Equation (2.17) is called the *kinematic boundary condition* [WCM03]. The physical meaning of this equation is that the flux of the velocity field $\mathbf{u_s^{(3)}}$ through the surface defined by $z = h$ is vanishing. Accordingly, we can define an arbitrary flux j through the free surface of the film as

$$j = \mathbf{e_n^{(3)}}\cdot(\mathbf{u}^{(3)}(\mathbf{x}, h(\mathbf{x}, t), t) - \mathbf{u_s}^{(3)}(\mathbf{x}, h(\mathbf{x}, t), t)). \tag{2.18}$$

Here, $\mathbf{e_n}^{(3)}$ is the normal vector to the surface of the film at $z = h$ as shown in figure 2.1. Now, we need to write the normal vector $\mathbf{e_n^{(3)}}$, as well as the tangential vectors $\mathbf{e_{tx}^{(3)}}$ and $\mathbf{e_{ty}^{(3)}}$, in an explicit form. Note that the surface at $z = h$ is given by the graph of the function $h(\mathbf{x})$. In this case the unit vectors locally normal or tangential with respect to the surface read

$$\mathbf{e_n^{(3)}} = \frac{1}{\sqrt{1 + (\partial_x h)^2 + (\partial_y h)^2}}(-\partial_x h, -\partial_y h, 1), \tag{2.19}$$

$$\mathbf{e_{tx}^{(3)}} = \frac{1}{\sqrt{1 + (\partial_x h)^2}}(1, 0, \partial_x h); \quad \mathbf{e_{ty}^{(3)}} = \frac{1}{\sqrt{1 + (\partial_y h)^2}}(0, 1, \partial_y h). \tag{2.20}$$

It is easily seen by rescaling that the normalization of these vectors is close to unity in the system we are interested in. We insert the above definition of the normal vector in equation (2.18). By performing the rescaling outlined in (2.13), combined with $j = \frac{h_0}{t_0}\tilde{j}$ and dropping the tildes, we obtain:

$$\mathbf{u_s} \cdot \boldsymbol{\nabla} h - u_{s.z} = j + \mathbf{u} \cdot \boldsymbol{\nabla} h - u_z. \tag{2.21}$$

As already suggested above, here we used the approximation $\frac{1}{\sqrt{1+\epsilon^2(\partial_{\tilde{x}}\tilde{h})^2+\epsilon^2(\partial_{\tilde{y}}\tilde{h})^2}} \approx 1$. We now insert (2.21) in (2.17) and the result in (2.16):

$$\partial_t h + \mathbf{u} \cdot \boldsymbol{\nabla} h = -\int_0^h \boldsymbol{\nabla} \cdot \mathbf{u} - j \Leftrightarrow \partial_t h = -\boldsymbol{\nabla} \cdot \int_0^h \mathbf{u}\, dz - j \tag{2.22}$$

$$\Leftrightarrow \partial_t h = -\boldsymbol{\nabla} \cdot (h\overline{\mathbf{u}}) - j. \tag{2.23}$$

Thus, the evolution equation of the height profile h in the thin film limit is an advection equation with the height averaged velocity field $\overline{\mathbf{u}}$ and a source term j defined by a rescaled version of equation (2.18). The source term j will obtain the physical meaning of an evaporation term later on.

2.2.2. Evolution of the Averaged Concentration

We will now proceed with the treatment of equations (2.7) and (2.11) with a diffusion coefficient given by the Einstein relation (2.11):

$$\rho(\partial_t c + \mathbf{u^{(3)}} \cdot \boldsymbol{\nabla}^{(3)} c) = -\boldsymbol{\nabla}^{(3)} \cdot \left(\rho \frac{k_B T}{6\pi a \eta} \boldsymbol{\nabla}^{(3)} c\right). \tag{2.24}$$

In order to use assumption (a), we start out by the nondimensionalization of equation (2.7). For this purpose, we use the scaling (2.13) and define

$$\eta = \eta_0 \tilde{\eta}; \qquad D = \frac{k_B T}{6\pi a \eta_0} \tilde{D} =: D_0 \tilde{D}. \tag{2.25}$$

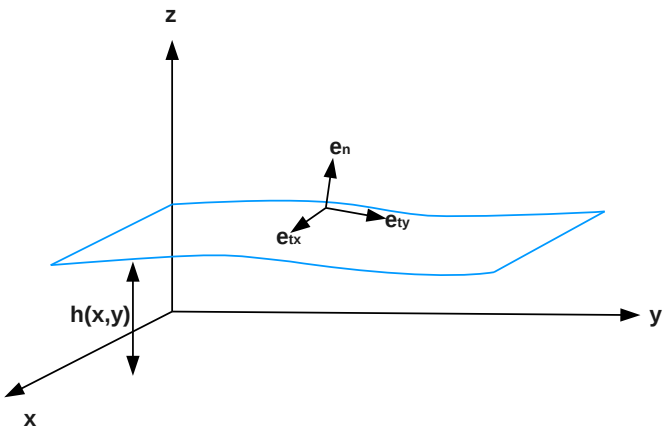

Figure 2.1.: Sketch of the height profile showing the choice the coordinate system used in the derivations as well as the normal and tangential unit vectors.

We insert the above scaling in (2.7), where we once again consider ρ to be approximately constant. Omitting the tildes, equation (2.7) can be written in a nondimensional form as

$$\frac{1}{t_0}\partial_t c + \frac{l_0}{t_0}\frac{\epsilon}{h_0}\mathbf{u}\cdot\boldsymbol{\nabla}c + \frac{h_0}{t_0}\frac{1}{h_0}u_z\partial_z c = \frac{\epsilon^2}{h_0^2}D_0\boldsymbol{\nabla}\cdot(D\boldsymbol{\nabla}C) + \frac{D_0}{h_0^2}\partial_z(D\partial_z c)$$
$$\Leftrightarrow \partial_t c + \mathbf{u}\cdot\boldsymbol{\nabla}c + u_z\partial_z c = \mathrm{Pe}^{-1}(\boldsymbol{\nabla}\cdot(D\boldsymbol{\nabla}c) + \frac{1}{\epsilon^2}\partial_z(D\partial_z c)). \tag{2.26}$$

The *Péclet number* $\mathrm{Pe} = \frac{u_0 l_0}{D_0}$ was defined, which is a dimensionless measure for the ratio of advective to diffusive transport rates [Pro05]. Now, the assumption (b) has to be quantified to be included in the derivations. The concentration is assumed to be only weakly dependent of the vertical space variable z and the following ansatz is performed:

$$c(\mathbf{x},z,t) = \phi(\mathbf{x},t) + \epsilon^2\mathrm{Pe}\ c_1(\mathbf{x},z,t), \quad \text{where} \quad \frac{1}{h}\int_0^h c(\mathbf{x},z,t)dz = \phi(\mathbf{x},z,t). \tag{2.27}$$

The parameter of smallness associated with the z-dependent part of c is chosen to be the vertical Péclet number $\mathrm{Pe}_z := \epsilon^2\mathrm{Pe}$. We can now insert the ansatz (2.27) into equation (2.26):

$$\partial_t\phi + \epsilon^2\mathrm{Pe}\ \partial_t c_1 + \mathbf{u}\cdot\boldsymbol{\nabla}\phi + \epsilon^2\mathrm{Pe}\ \mathbf{u}\cdot\boldsymbol{\nabla}c_1 + \epsilon^2\mathrm{Pe}\ u_z\partial_z c_1 \tag{2.28}$$
$$= \mathrm{Pe}^{-1}(\boldsymbol{\nabla}\cdot(D\boldsymbol{\nabla}\phi) + \epsilon^2\mathrm{Pe}\boldsymbol{\nabla}\cdot(D\boldsymbol{\nabla}c_1) + \mathrm{Pe}\ \partial_z(D\partial_z c_1)).$$

Assuming that Pe is of order $\mathcal{O}(1)$, we obtain, when neglecting terms of order $\mathcal{O}(\epsilon^2)$,

$$\partial_t c_0 + \mathbf{u}\cdot\boldsymbol{\nabla}c_0 = \mathrm{Pe}^{-1}(\boldsymbol{\nabla}\cdot(D\boldsymbol{\nabla}c_0) + \mathrm{Pe}\ \partial_z(D\partial_z c_1)). \tag{2.29}$$

Furthermore, up to $\mathcal{O}(\epsilon^2)$, we can perform the expansion

$$D(\phi + \epsilon^2 \mathrm{Pe} c_1) = D(\phi) + \epsilon^2 \mathrm{Pe} c_1 D'(\phi) = D(\phi) + \mathcal{O}(\epsilon^2). \tag{2.30}$$

Finally, averaging equation (2.29) according to $\overline{f} = \frac{1}{h}\int_0^h f dz$ yields

$$\begin{aligned} \partial_t \phi + \overline{\mathbf{u}} \cdot \boldsymbol{\nabla} c_0 &= \mathrm{Pe}^{-1} \boldsymbol{\nabla} \cdot (D \boldsymbol{\nabla} \phi) + \frac{1}{h} \int_0^h \partial_z (D \partial_z c_1) dz \\ \Leftrightarrow \partial_t \phi + \overline{\mathbf{u}} \cdot \boldsymbol{\nabla} \phi &= \mathrm{Pe}^{-1} \boldsymbol{\nabla} \cdot (D \boldsymbol{\nabla} \phi) + \frac{D}{h} ((\partial_z c_1)|_{z=h} - (\partial_z c_1)|_{z=0}). \end{aligned} \tag{2.31}$$

To close this equation, we need boundary conditions for $z = 0$ and $z = h$, respectively and an expression for the averaged velocity field $\overline{\mathbf{u}} = \frac{1}{h}\int_0^h \mathbf{u}\, dz$ which is to be derived from the Navier-Stokes equation, as already mentioned.

Boundary at the substrate

For the boundary at $z = 0$, we assume that the diffusive flux $\mathbf{J_{diff}} = -D(c)\boldsymbol{\nabla}^{(3)} c$ vanishes in the direction of the substrate (i.e., in the direction $-\mathbf{e_z^{(3)}}$). The advective flux vanishes due to the no-penetration boundary condition, which will be used to solve the Navier-Stokes equation. This leads directly to the relation:

$$D(\phi)\partial_z c_1(\mathbf{x}, z = 0) = 0. \tag{2.32}$$

It has to be emphasized that a different ansatz could be chosen at $z = 0$, assuming that the diffusive flux at the $z = 0$ is equal to a deposition rate of the solute on the substrate. For a deposition rate linear in c, this would lead to the boundary condition

$$D\partial_z c_1 \propto \phi. \tag{2.33}$$

Boundary at the free surface

The physical idea behind the boundary condition at the free surface ($z = h$) is that no solute should leave the film through this surface. According to equation (2.18), we can write the advective flux of solute through the surface as $j_{ad} = c\, \mathbf{e_n^{(3)}} \cdot (\mathbf{u}(\mathbf{x}, h(\mathbf{x}, t), t) - \mathbf{u_s}(\mathbf{x}, h(\mathbf{x}, t), t)) = c\ j$. We then obtain the yet to be nondimensionalized boundary condition:

$$j\ c|_{z=h} - (D\ \mathbf{e_n^{(3)}} \cdot \boldsymbol{\nabla}^{(3)} c)|_{z=h} = 0. \tag{2.34}$$

$$\tag{2.35}$$

We insert the definition (2.20) of the normal vector into the boundary condition above. The resulting equation can be rescaled in an analogous way as in (2.21).

Once again, we immediately omit the tildes:

$$jc|_{z=h} = -\frac{1}{\mathrm{Pe}} D\boldsymbol{\nabla} c \cdot \boldsymbol{\nabla} h|_{z=h} + \frac{1}{\epsilon^2 \mathrm{Pe}} D\partial_z c|_{z=h} \tag{2.36}$$

Now, including the decomposition (2.27) yields:

$$\begin{aligned} j\phi|_{z=h} + jc_1\epsilon^2\mathrm{Pe}|_{z=h} &= -\frac{1}{\mathrm{Pe}} D\boldsymbol{\nabla} h \cdot \boldsymbol{\nabla}\phi - \epsilon^2 D\boldsymbol{\nabla} h \cdot \boldsymbol{\nabla} c_1|_{z=h} + D\partial_z c_1|_{z=h} \\ &\underset{\mathcal{O}(\epsilon)}{\Rightarrow} D\partial_z c_1|_{z=h} = j\phi + \frac{1}{\mathrm{Pe}} D\boldsymbol{\nabla} h \cdot \boldsymbol{\nabla}\phi. \end{aligned} \tag{2.37}$$

The boundary conditions (2.32) and (2.37) can now be inserted into equation (2.31):

$$\begin{aligned} &\partial_t \phi + \overline{\mathbf{u}} \cdot \boldsymbol{\nabla}\phi = \mathrm{Pe}^{-1} \boldsymbol{\nabla}(D\boldsymbol{\nabla}\phi) + \frac{1}{h}(j\phi + \mathrm{Pe}^{-1} D\boldsymbol{\nabla} h \cdot \boldsymbol{\nabla}\phi) \\ \Leftrightarrow\ &\partial_t \phi + \overline{\mathbf{u}} \cdot \boldsymbol{\nabla}\phi = \frac{1}{h}\left(\frac{1}{\mathrm{Pe}}(\boldsymbol{\nabla}(hD\boldsymbol{\nabla}\phi)) + j\phi\right). \end{aligned} \tag{2.38}$$

2.2.3. Lubrication approximation of the Navier-Stokes equation

We now need to compute an expression for the height averaged velocity field in the thin film geometry. This can be achieved by solving the Navier-Stokes equation in the framework of a long-wave expansion, subjected to appropriate boundary conditions. The scaling and approximations presented here, as well as the treatment of the boundary conditions shown in the next section, follow the derivations carried out in [Köp11]. The incompressible Navier-Stokes equation has to be written with a non constant viscosity $\eta = \eta(\phi + \epsilon^2 \mathrm{Pe}\ c_1)$. Since we will only consider the lowest order terms in ϵ, at this point, we can introduce the approximation $\eta\left(c\left(\mathbf{x}, z\right)\right) \approx \eta(\phi(\mathbf{x}, t)) + \epsilon^2 \mathrm{Pe}\ \eta'(\phi(\mathbf{x}, t))\ c_1(\mathbf{x}, z, t) \approx \eta(\phi)$ and obtain:

$$\rho(\partial_t \mathbf{u^{(3)}} + \mathbf{u^{(3)}} \cdot \boldsymbol{\nabla}\mathbf{u^{(3)}}) = -\boldsymbol{\nabla}^{(3)} p + \boldsymbol{\nabla}^{(3)} \cdot \boldsymbol{\gamma} \tag{2.39}$$

$$(\boldsymbol{\nabla}^{(3)} \cdot \boldsymbol{\gamma})_i = \partial_{x_k}\left(\eta(\phi)\left(\partial_{x_k}\partial u_i\right) + \partial_{x_i} u_k\right) = \partial_{x_k} u_i \partial_{x_k}\eta + \partial_{x_i} u_k \partial_{x_k}\eta + \eta\Delta^{(3)} u_i \tag{2.40}$$

We now first consider the equation for $\mathbf{u}$. It is rescaled according to the scaling (2.13), completed with the scaling $p = \frac{t_0\epsilon^2}{\eta}\tilde{p}$ of the pressure terms and the introduction of the classical *Reynolds number* $\mathrm{Re} = \frac{\rho l_0 h_0}{\eta t_0}$. The scaling of the pressure terms might seem ad hoc at this point, but we will see later that the scaling corresponds to an assumed relationship of time and energy scales. The nondimensional Navier-Stokes equation for $\mathbf{u}$ reads without tildes:

$$\partial_t \mathbf{u} + (\mathbf{u} \cdot \boldsymbol{\nabla} + u_z \partial_z)\mathbf{u} = \mathrm{Re}^{-1}\left(\epsilon\eta\Delta\mathbf{u} + \epsilon^{-1}\eta\partial_z^2\mathbf{u} + \epsilon\boldsymbol{\nabla}\eta \cdot \boldsymbol{\nabla}\mathbf{u} + \epsilon\boldsymbol{\nabla}u_k \cdot \boldsymbol{\nabla}\eta - \epsilon^{-1}\boldsymbol{\nabla}p\right). \tag{2.41}$$

Here we used the approximation $\eta \approx \eta(\phi)$ and thus $\partial_z \eta \approx 0$. Furthermore, the notations $x_1 = x,\ x_2 = y,\ x_3 = z$ were used. Then, for the lowest order in ϵ, we obtain:

$$\eta \partial_z^2 \mathbf{u} = \boldsymbol{\nabla} p. \tag{2.42}$$

For the z component of the velocity analogous calculations lead to

$$\partial_t u_z + (\mathbf{u} \cdot \boldsymbol{\nabla} + u_z \partial_z) u_z = \mathrm{Re}^{-1} \left(\epsilon \eta \Delta u_z + \epsilon \boldsymbol{\nabla} u_z \cdot \boldsymbol{\nabla} \eta + \epsilon^{-1} (\partial_z \mathbf{u}) \cdot \boldsymbol{\nabla} \eta - \epsilon^{-3} \partial_z p \right). \tag{2.43}$$

That is, in lowest order in ϵ only one term remains and the two equations resulting from the lubrication approximation of the Navier-Stokes equation are

$$\eta \partial_z^2 \mathbf{u} = \boldsymbol{\nabla} p, \tag{2.44}$$

$$\partial_z p = 0. \tag{2.45}$$

Obviously, the simplifications are very drastic and one arrives at the same result when one simply starts from the Stokes equation arguing that inertial effects are negligible for very thin films. Nevertheless, it is instructive to see how one arrives at the same equations starting with the Navier-Stokes equation in a very general form when using the appropriate ansatz for the concentration field $c(\mathbf{x}, z)$.

2.3. Boundary conditions for the thin film flow

To solve equations (2.44) and (2.45), once again boundary conditions for the boundaries at $z = 0$ (boundary at the substrate) and at $z = h$ have to be provided. For the boundary condition at the substrate we choose the so-called *no-slip boundary condition*, i.e., the velocity of the fluid flow at the substrate has to be equal to the velocity $\mathbf{v}$ of the substrate:

$$\mathbf{u}(\mathbf{x}, z = 0) = \mathbf{v}. \tag{2.46}$$

The boundary condition at the free surface is more complicated and its formulation necessitates an appropriate description of the forces at the surface. As a first step we will formulate the boundary conditions for the general case and will then apply the lubrication approximation to obtain the boundary conditions for equations (2.44) and (2.45). Following [LLW91], we consider a film where the surface is infinitesimally changed by δf and the height is changed by δz. Now, there are two different types of forces acting on the film during the change of geometry described above. The first type of force is due to the well known surface tension σ of the film and the change in the energy due to this force can be written as $\delta E_{\text{surface}} = \sigma \delta f$.
The second type of force is due to the difference between the pressure p_l in the liquid and the pressure p_g in the gas phase. The respective force acting on an infinitesimal part df of the surface of the film is $(p_l - p_g) df$.

At this point, we need to introduce a physical quantity which becomes meaningful and important for the description of thin liquid films on a substrate: the *disjoining pressure* Π, which was first introduced by Derjaguin [Der40]. The disjoining pressure is used to describe the interaction of the liquid and the substrate and is explicitly dependent on the height h of the film. It typically consists of a long range attractive term and a short range repulsive term, our particular choice and further possible choices of the disjoining pressure will be discussed in chapter 4. For now, it is important to know that the disjoining pressure has to be included in the considerations as a supplement to the pressure p_l. Altogether, the overall energy change δE due to the deformation $(\delta z, \delta f)$ can be written as

$$\delta E = -\int (p_l - \Pi - p_g)\delta z df + \sigma \delta f. \tag{2.47}$$

We now want to express the change δf of the surface in dependence of the infinitesimal change of the height δz. Locally the non-flat surface df can be described through the two main radii of curvature κ_1, κ_2. Up to the first order in δz, the surface element df is changed as $df \to \delta z df(\kappa_1 + \kappa_2)$ and thus we can write:

$$\delta E = -\int \delta z \left[p_l - \Pi - p_g - \sigma(\kappa_1 + \kappa_2)\right] df. \tag{2.48}$$

In equilibrium, the change in energy has to vanish for all infinitesimal changes δz. From this requirement we obtain the famous *Laplace equation* supplemented with the disjoining pressure term:

$$p_l - p_g = \Pi + \sigma(\kappa_1 + \kappa_2). \tag{2.49}$$

This equation can be used to formulate a condition for the stresses acting upon the free surface. In general, the following relation between the stress tensor $\boldsymbol{\tau}$, the viscous stress tensor $\boldsymbol{\gamma}$ and the pressure holds in a continuous medium:

$$\tau_{ij} = -p\ \delta_{ik} + \gamma_{ij} = -p\ \delta_{ij} + \eta\left(\partial_{x_j} u_i + \partial_{x_j} u_j\right). \tag{2.50}$$

Here and in the following, the indices are elements of $\{1, 2, 3\}$. The vector valued stresses acting on a surface with normal vector $\mathbf{n^{(3)}}$ can be expressed in terms of the stress tensor by

$$\boldsymbol{\tau} \cdot \mathbf{n^{(3)}}|_{\text{surface}} := \tau_{ij} n_j|_{\text{surface}}. \tag{2.51}$$

Assuming that the difference of the viscous stresses of liquid and gas at the surface vanishes and using equation (2.44), we obtain for the difference of the stresses acting on the surface which has the normal vector $\mathbf{e_n^{(3)}}$:

$$-\Pi\ \mathbf{e_n^{(3)}} - \sigma(\kappa_1 + \kappa_2)\mathbf{e_n^{(3)}} = \left((\boldsymbol{\tau_l} - \boldsymbol{\tau_g}) \cdot \mathbf{e_n^{(3)}}\right)\Big|_{z=h} \approx \left(\boldsymbol{\tau_l} \cdot \mathbf{e_n^{(3)}}\right)\Big|_{z=h}. \tag{2.52}$$

The above approximation is valid because the stresses in a gaseous phase are in general much smaller than in the liquid phase.
Finally, to obtain the boundary conditions for the Navier-Stokes equation at the free surface, we can project equation (2.52) on the directions of the unit vectors normal and tangential to the surface defined in equation (2.20):

$$\left(\mathbf{e_n^{(3)}} \cdot \boldsymbol{\tau_l} \cdot \mathbf{e_n^{(3)}}\right)\Big|_{z=h} = -\Pi - \sigma(\kappa_1 + \kappa_2), \tag{2.53}$$

$$\left(\mathbf{e_{tx}^{(3)}} \cdot \boldsymbol{\tau_l} \cdot \mathbf{e_n^{(3)}}\right)\Big|_{z=h} = 0 = \left(\mathbf{e_{ty}^{(3)}} \cdot \boldsymbol{\tau} \cdot \mathbf{e_n^{(3)}}\right)\Big|_{z=h}. \tag{2.54}$$

These boundary conditions can now be nondimensionalized using the same scaling as in section 2.2.3. As the appearing terms are quite extensive, we only write down the resulting equations up to lowest order in ϵ for the boundary conditions (2.54) and for the first two orders of ϵ for the boundary condition (2.53). As usual, we immediately omit the tildes and obtain:

$$\left(\mathbf{e_{tx}^{(3)}} \cdot \boldsymbol{\tau_l} \cdot \mathbf{e_n^{(3)}}\right)\Big|_{z=h} = 0 \quad \longrightarrow \quad \left(\frac{\eta\eta_0}{t_0\epsilon}\partial_z u_x\right)\Big|_{z=h} = 0, \tag{2.55}$$

$$\left(\mathbf{e_{ty}^{(3)}} \cdot \boldsymbol{\tau_l} \cdot \mathbf{e_n^{(3)}}\right)\Big|_{z=h} = 0 \quad \longrightarrow \quad \left(\frac{\eta\eta_0}{t_0\epsilon}\partial_z u_y\right)\Big|_{z=h} = 0, \tag{2.56}$$

$$\left(\mathbf{e_n^{(3)}} \cdot \boldsymbol{\tau_l} \cdot \mathbf{e_n^{(3)}}\right)\Big|_{z=h} = -\Pi - \sigma(\kappa_1 + \kappa_2) \quad \longrightarrow \quad 0 = \left(\frac{\eta}{t_0\epsilon^2}(\Pi - p) - \frac{h_0\sigma}{l_0^2}\Delta h\right)\Big|_{z=h}. \tag{2.57}$$

We take advantage of the fact that the curvatures κ_1 and κ_2 of a surface given by the graph of $h(\mathbf{x})$ can be approximated through the second derivatives of h with respect to x and y ($\kappa_1 + \kappa_2 \approx -(\partial_x^2 h + \partial_y^2 h)$). Equations (2.55)-(2.57) can now be introduced as boundary conditions to the equations (2.44) and (2.45). The latter can then be solved easily. By integrating equation (2.44) twice with respect to z, we obtain:

$$\eta\mathbf{u} = \frac{1}{2}z^2\boldsymbol{\nabla}p + \mathbf{a_1}z + \mathbf{a_2} \tag{2.58}$$

Once again, we used the approximation $\eta \approx \eta(\phi)$ and thus the approximate independence of η with respect to z. From $\partial_z\mathbf{u}|_{z=h} = 0$ and equation (2.45), we can deduce $\mathbf{a_1} = -(h\boldsymbol{\nabla}p)|_{z=h}$ and the no slip boundary condition leads to $\mathbf{a_2} = \eta\mathbf{v}$. Hence, we can conclude:

$$\mathbf{u}(\mathbf{x}, z = h, t) = -\frac{h^2}{2\eta}\boldsymbol{\nabla}(\Pi - \epsilon^3\mathrm{Ca}^{-1}\Delta h) + \mathbf{v} \tag{2.59}$$

$$\Rightarrow \overline{\mathbf{u}} = \frac{1}{h}\int_0^h \mathbf{u}dz = -\frac{h^2}{3\eta}\boldsymbol{\nabla}\overline{p} + \mathbf{v}; \quad \overline{p} := \Pi - \epsilon^3\mathrm{Ca}^{-1}\Delta h \tag{2.60}$$

Here, we introduced the dimensionless parameter $\mathrm{Ca} = \frac{l_0 \eta_0}{t_0 \sigma}$, which is well known in literature as the *Capillary number* and is a measure for the ratio between viscous and surface forces [Pro05]. We are now in the position to close the evolution equations for the averaged concentration field and the height profile which will be the starting point for further considerations in this work:

$$\partial_t h = -\boldsymbol{\nabla} \cdot (\mathbf{J}_{\mathrm{adv}}) - j - \boldsymbol{\nabla} h \cdot \mathbf{v}, \tag{2.61}$$

$$\partial_t \phi = -\frac{1}{h} \mathbf{J}_{\mathrm{adv}} \cdot \boldsymbol{\nabla} \phi + \frac{1}{h} \left(\frac{1}{\mathrm{Pe}} (\boldsymbol{\nabla} (h D \boldsymbol{\nabla} \phi)) + j \phi \right) - \boldsymbol{\nabla} \phi \cdot \mathbf{v}, \tag{2.62}$$

$$\text{where} \qquad \mathbf{J}_{\mathrm{adv}} := -\frac{h^3}{3\eta(\phi)} \boldsymbol{\nabla} \overline{p}. \tag{2.63}$$

3. Free Energy Approach to Relaxational Dynamics

In this chapter, we will first reformulate the simple diffusion equation using a free energy functional. This approach will then be extended to obtain a PDE for a system exhibiting phase separation and so-called *uphill diffusion*. Finally, we will show that the conservative part of our basic equations (2.61) and (2.62) can also be formulated in a similar way.

3.1. Diffusion Equation and Cahn-Hilliard Free Energy

In classical thermodynamics, the Helmholtz free energy is defined as [Hil60]

$$F = U - TS, \tag{3.1}$$

where U is the inner energy of the system, T is the temperature and S is the entropy. The concept of a free energy can be extended to spatially inhomogeneous binary systems characterized through local concentrations[1], and can be used to derive equations for the spatio-temporal dynamics of those systems.
We introduce a free energy functional $\mathcal{F}[c]$ as the integral of a free energy density over the volume Ω of the considered system:

$$\mathcal{F}[c] = \int_{\Omega} f(c, \boldsymbol{\nabla} c, ..) dx^n. \tag{3.2}$$

The free energy density $f(c, \boldsymbol{\nabla} c, ..)$ is locally dependent on the concentration and derivatives of the concentration, respectively. By means of a functional derivative of the free energy functional with respect to the concentration, we define a *generalized chemical potential* μ_c [God91]. The corresponding *chemical force* $\mathbf{F}_c$ is given by the negative gradient of this potential:

$$\mathbf{F}_c = -\boldsymbol{\nabla} \mu_c = -\boldsymbol{\nabla} \frac{\delta \mathcal{F}}{\delta c}. \tag{3.3}$$

We now assume that the flux of the concentration can be expressed through a, in general concentration-dependent, *mobility coefficient* $M(c)$ and the chemical force:

$$\mathbf{J}_c = M(c)\ \mathbf{F}_c = -M(c)\ \boldsymbol{\nabla} \frac{\delta \mathcal{F}}{\delta c}. \tag{3.4}$$

[1] Here and in the following by concentration we mean per volume concentration of one of the components.

The continuity equation for the concentration then reads

$$\partial_t c = -\boldsymbol{\nabla} \cdot \mathbf{J_c} = \boldsymbol{\nabla} \cdot \left(M(c)\ \boldsymbol{\nabla} \frac{\delta \mathcal{F}}{\delta c} \right). \tag{3.5}$$

For positive mobility coefficients $M(c) > 0,\ \forall c \in [0,1]$ and vanishing fluxes through the surface of the volume Ω, the free energy functional is a *Lyapunov functional* of equation (3.5), i.e., a functional which is minimized for stationary solutions of the equation [Pis06]:

$$\begin{aligned} \frac{d}{dt}\mathcal{F} &= \int\limits_{\Omega} \frac{\delta \mathcal{F}}{\delta c(\mathbf{x}')} \partial_t c(\mathbf{x}')\ dx'^n = \int\limits_{\Omega} \frac{\delta \mathcal{F}}{\delta c(\mathbf{x}')} \boldsymbol{\nabla} \cdot \left(M(c(\mathbf{x}'))\ \boldsymbol{\nabla} \frac{\delta \mathcal{F}}{\delta c(\mathbf{x}')} \right)\ dx'^n \\ &= -\int\limits_{\Omega} M(c(\mathbf{x}')) \left(\boldsymbol{\nabla} \frac{\delta \mathcal{F}}{\delta c(\mathbf{x}')} \right)^2 dx'^n \leq 0. \end{aligned} \tag{3.6}$$

An almost trivial example is a binary mixture exhibiting purely diffusional dynamics for small concentrations. We formulate the following free energy functional of purely entropic type for this system:

$$\mathcal{F}[c] = \int\limits_{V} dx^3 \frac{k_\mathrm{B} T}{a^3}\ c\ \ln(c). \tag{3.7}$$

The diffusion equation with a diffusion coefficient following the Einstein relation (2.11) can be written in terms of the free energy functional and a mobility coefficient $M(c) = \frac{c\ a^2}{6\pi\eta}$:

$$\partial_t c = \boldsymbol{\nabla} \cdot \left[M(c) \boldsymbol{\nabla} \frac{\delta \mathcal{F}}{\delta c} \right] = D\ \Delta c. \tag{3.8}$$

For interacting particles, a dependence of the free energy on concentration gradients should be expected for inhomogeneous systems. In [CH58], Cahn and Hilliard were able to derive a free energy density exhibiting a dependence on gradients in the most simple form by symmetry arguments. The arguments used in [CH58] are based on a Taylor expansion of a free energy density about the free energy density of a homogeneous system $f_0(c)$:

$$f(c, \partial_{x_i} c, \partial_{x_i}\partial_{x_j} c) \approx f_0(c) + G_i\ \partial_{x_i} c + \kappa'_{ij}\ \partial^2_{x_i x_j}\ c + \kappa''_{ij} \partial_{x_i} c\ \partial_{x_j} c. \tag{3.9}$$

The assumption was used that interactions of the particles in the system are sufficiently local, so that gradient contributions of higher order can be neglected. Now, the free energy density has to be invariant to the operations $R_1 : x_i \to -x_i$ (reflection) and $R_2 : x_i \to x_j$ (rotation) in order to account for an isotropic system. The expression for the free energy density (3.9) therefore reduces to

$$f(c, \partial_{x_i} c, \partial_{x_i}\partial_{x_j} c) \approx f_0(c) + \kappa' \Delta c + \kappa'' \left(\boldsymbol{\nabla} c \right)^2. \tag{3.10}$$

The second and third term can finally be combined due to Green's theorem, if we assume a vanishing flux through the boundary of the volume. Using the expression $\kappa = -\frac{d}{dc}\kappa' + \kappa''$, we obtain:

$$f(c, \boldsymbol{\nabla} c) = f_0(c) + \kappa(\boldsymbol{\nabla} c)^2. \tag{3.11}$$

The *Cahn-Hilliard equation* in the most general form is obtained by inserting the Cahn-Hilliard free energy (3.11) into (3.5):

$$\partial_t c = \boldsymbol{\nabla} \cdot \left(M(c)\ \boldsymbol{\nabla} \frac{\delta \mathcal{F}}{\delta c} \right) = \boldsymbol{\nabla} \cdot \left(M(c)\ \boldsymbol{\nabla} \left(\frac{\partial f_0}{\partial c} - \kappa \Delta c \right) \right). \tag{3.12}$$

For a certain class of free energy densities $f_0(c)$, the solutions to this equation show the dynamics of *phase separation* as well as *coarsening* of phase separated structures. Before the discussion of these dynamics, it is instructive to revise shortly some aspects of a thermodynamical (equilibrium) theory of stability and phase separation.

3.2. Thermodynamics of Phase Separation

The most prominent example of a theory describing the thermodynamics of phase separation is the van der Waals theory for real gases. The well known equation of state reads [LL70]

$$\left(p + \frac{a}{v^2} \right) (v - b) = k_\mathrm{B} T. \tag{3.13}$$

Here, p is the pressure of the gas, $v = V/N$ is defined by the total volume V and the number of particles N as the specific volume occupied by a particle. The constants a and b arise from particle interactions and the finite extent of the particles. The corresponding Helmholtz free energy (3.1) can be rescaled by the number of particles N to obtain the specific free energy $\tilde{f} = \frac{F}{N}$ [Hil60]:

$$\tilde{f} = -k_\mathrm{B} T \left(1 + \ln \left(\frac{(v-b) T^{3/2}}{c} \right) \right) - \frac{a}{v}. \tag{3.14}$$

We consider a system described by (3.14), consisting of a fixed number of particles confined to a volume V_0. For the van der Waals gas, the specific volume $v = \frac{V}{N}$ can be considered as the *order parameter* allowing the differentiation between liquid and gaseous states. For the given system, we are now interested in the question if the phase separation occurs, i.e., if the overall free energy of the system in the homogeneous state $F_{hom} = N\tilde{f}(v = v_0)$ can be lowered through the separation of the system into a fraction N_I of particles with the specific volume v_I and a fraction N_II of particles with the specific volume v_II, respectively. The obvious constraints to $N_\mathrm{I,II}$ and $v_\mathrm{I,II}$ are

$$N_\mathrm{I} + N_\mathrm{II} = N; \quad N_\mathrm{I}\ v_\mathrm{I} + N_\mathrm{II}\ v_\mathrm{II} = v_0 N \tag{3.15}$$

$$\Rightarrow \quad N_\mathrm{I} = N \frac{v_\mathrm{II} - v_0}{v_\mathrm{II} - v_\mathrm{I}}; \quad N_\mathrm{II} = N \frac{v_0 - v_\mathrm{I}}{v_\mathrm{II} - v_\mathrm{I}}. \tag{3.16}$$

Thus, the free energy of the phase separated system reads:

$$F_{\text{inhom}} = N\left(\frac{v_{\text{II}} - v_0}{v_{\text{II}} - v_{\text{I}}} f(v_{\text{I}}) + \frac{v_0 - v_{\text{I}}}{v_{\text{II}} - v_{\text{I}}} f(v_{\text{II}})\right). \tag{3.17}$$

Equation (3.17) simply states that the free energy F_{inhom} resulting from a phase separation of a system initially characterized by the uniform order parameter v_0 is given by the value of the linear interpolation between the two phases evaluated at $v = v_0$. As it can be easily seen from geometrical considerations or variational calculus, the common tangent points of the free energy $\tilde{f}$ denoted by $v_{\text{I}}, v_{\text{II}}$ in figure 3.1 are the energetically most favorable phases for the decomposition. The decomposition into the phases v_{I} and v_{II} yields the lowest possible free energy for all initial order parameters v_0 located between v_{I} and v_{II}.
For order parameters $v_0 \notin [v_I, v_{\text{II}}]$, equation (3.17) implies that no energetically favorable inhomogeneous system exists. The region delimited by the coexisting phases v_{I} and v_{II} is called the *binodal region*. As stated above, the coexisting phases v_{I} and v_{II} are defined as the common tangent points of $\tilde{f}$. The corresponding equations determining the two values are

$$\tilde{f}'(v_{\text{I}}) = \tilde{f}'(v_{\text{II}}); \qquad \tilde{f}(v_{\text{I}}) + \tilde{f}'(v_{\text{I}})(v_{\text{II}} - v_{\text{I}}) = \tilde{f}(v_{\text{II}}). \tag{3.18}$$

Through a simple calculation (cf. [Köp11]), the conditions (3.18) can be reformulated to the well known thermodynamic conditions for phase coexistence:

$$p(V_{\text{I}}) = p(V_{\text{II}}); \qquad \mu(V_{\text{I}}, p_{\text{I}}) = \mu(V_{\text{II}}, p_{\text{II}}), \tag{3.19}$$

where μ is the chemical potential of each phase. One can furthermore note that the conditions (3.19) may be written in terms of the well known *Maxwell construction* (e.g [LL70]).
As a subset of the binodal region we now wish to identify the region where an infinitesimal change of the order parameter leads to a reduction of the free energy. This subset of the phase space is denoted as the *spinodal region* and here infinitesimal fluctuations of the order parameter induce phase separation. The calculations shown here follow along the lines of a similar derivation presented in [Köp11].
We once again consider a system consisting of N particles. Let a subset $\overline{N}$ of the particles be subject to fluctuations, such that the specific volume of a number $N_1 < \overline{N}$ of particles is augmented infinitesimally by dv. Due to the conservation constraint (3.16), the specific volume of the remaining $N_2 = \overline{N} - N_1$ particles needs to change by $dv_2 = -\frac{N_1 dv_1}{\overline{N} - N_1}$. The resulting free energy difference with respect to the unperturbed homogeneous state then reads

$$\begin{aligned}\Delta F &= N_1 f(v_0 + dv_1) + (\overline{N} - N_1) f\left(v_0 - \frac{N_1 dv_1}{N_2}\right) - \overline{N} f(v_0) \\ &= \left(\frac{N_1}{2} + \frac{N_1^2}{2(\overline{N} - N_1)}\right)(dv_1)^2 \left.\frac{\partial^2 f}{\partial v^2}\right|_{v=v_0} + \mathcal{O}((dv_1)^3).\end{aligned} \tag{3.20}$$

The first factor in equation (3.20) is non-negative per construction. Thus, the free energy is lowered through an infinitesimal fluctuation for all $v_0 \in \left\{ v_0 \;\middle|\; \frac{\partial^2 f}{\partial v^2}\Big|_{v=v_0} < 0 \right\}$. In the thermodynamical context, this is the range of specific volumes, where the isothermal compressibility is negative and the system is thus mechanically unstable. Homogeneous systems in the spinodal region can be considered unstable. Outside of the spinodal region and inside the binodal region, homogeneous states are denoted as *metastable*, i.e., their free energy is lowered by phase separation, but infinitesimal fluctuations do not suffice to induce the separation. Here phase separation does not occur due to *spinodal decomposition* triggered by fluctuations but through *nucleation* (see e.g. [CH59]). In the (p, v_0) phase diagram for the van der Waals gas, the limits of the spinodal and binodal regions meet for the critical temperature at $T = T_C$. For temperatures $T > T_C$, no phase separation occurs.

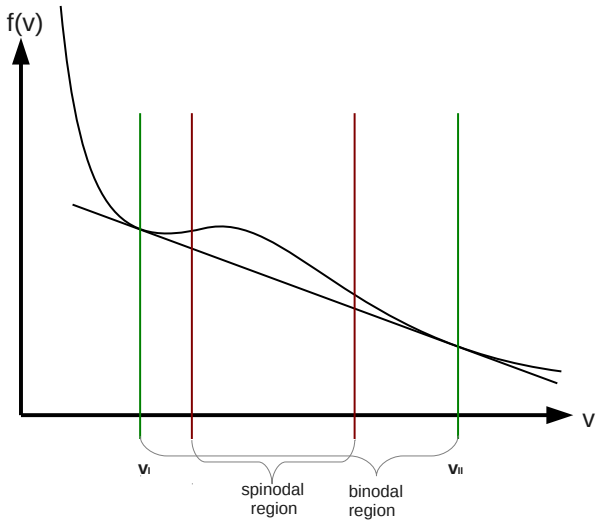

Figure 3.1.: Sketch of the specific free energy of a van der Waals gas. The limits of the binodal region (green) and spinodal region (red) are shown as well as the coexisting specific volumes $v_{\mathrm{I}}, v_{\mathrm{II}}$ and the respective common tangent.

3.3. Dynamics of the Cahn-Hilliard Equation

We return to the discussion of the Cahn-Hilliard equation (3.12). We already noted that for a closed system of volume Ω, the free energy functional is a Lyapunov functional of the PDE and the solutions of equation (3.12) will evolve towards a minimum of $\mathcal{F}$. Performing the mapping $N \to \Omega$, and $v \to c$, the arguments related to equations (3.17), (3.20) which were presented in the previous section can be formulated analogously for the free energy

$$\tilde{\mathcal{F}}[c] = \int_{\Omega} dx^n f_0(c(\mathbf{x})). \tag{3.21}$$

The concentration c is now the conserved order parameter. Let the local free energy density $f_0(c)$ exhibit double tangent points $c_{\mathrm{I}}, c_{\mathrm{II}}$. We then expect homogeneous solutions $c(\mathbf{x}) = c_0$ of equation (3.12) to be unstable, if c_0 is in the spinodal region $\left(\frac{\partial^2 f}{\partial c^2}|_{c=c_0} < 0\right)$, and phase separation into domains of concentration c_{I} and domains of concentration c_{II} to occur. This instability is readily confirmed by a linear stability analysis of equation (3.12). We perform the ansatz $c(\mathbf{x}, t) = c_0 + \eta(\mathbf{x}, t)$ [NCS84]:

$$\begin{aligned} \partial_t\, \eta(\mathbf{x}, t) &= \boldsymbol{\nabla} M(c) \cdot \boldsymbol{\nabla} \left(f_0'(c) - \kappa \Delta c \right) + M(c) \Delta \left(\left. \frac{\partial f_0}{\partial c} \right|_{c=c_0+\eta} - \kappa \Delta c \right) \\ &= M(c_0) \left(\left. \frac{\partial^2 f_0}{\partial c^2} \right|_{c=c_0} \Delta \eta - \Delta^2 \eta \right) + \mathcal{O}(\eta^2). \end{aligned} \tag{3.22}$$

To investigate the linear stability with respect to undulations, we furthermore assume $\eta(\mathbf{x}, t) = \eta_{\mathbf{k}}\, e^{i\mathbf{k}\cdot\mathbf{x} + \nu(\mathbf{k})}$. This ansatz yields the isotropic dispersion relation

$$\nu(k) = M(c_0) \left(- \left. \frac{\partial^2 f_0}{\partial c} \right|_{c=c_0} k^2 - \kappa k^4 \right) \tag{3.23}$$

As one can see from equations (3.22) and (3.23), the curvature $\left. \frac{\partial^2 f_0}{\partial c} \right|_{c=c_0}$ determines the sign of the diffusion coefficient in the linear regime. The linear diffusion coefficient becomes negative for the already thermodynamically derived condition $\frac{\partial^2 f}{\partial c}|_{c=c_0} < 0$. In this case, phase separation into the coexisting phases occurs through so-called *uphill diffusion*. The Cahn-Hillard equation reflects the spinodal instability of the free energy as a linear instability of the corresponding homogeneous solutions. Through the dispersion relation (3.23), the role of the biharmonic term in the Cahn Hilliard equation (3.12) is also clarified. For a negative curvature of f_0, the term leads to the stabilization of high wavenumbers, as shown in figure 3.4. In the free energy functional, the biharmonic term corresponds to the gradient contribution. High gradients lead to an increase of the free energy and are therefore suppressed.

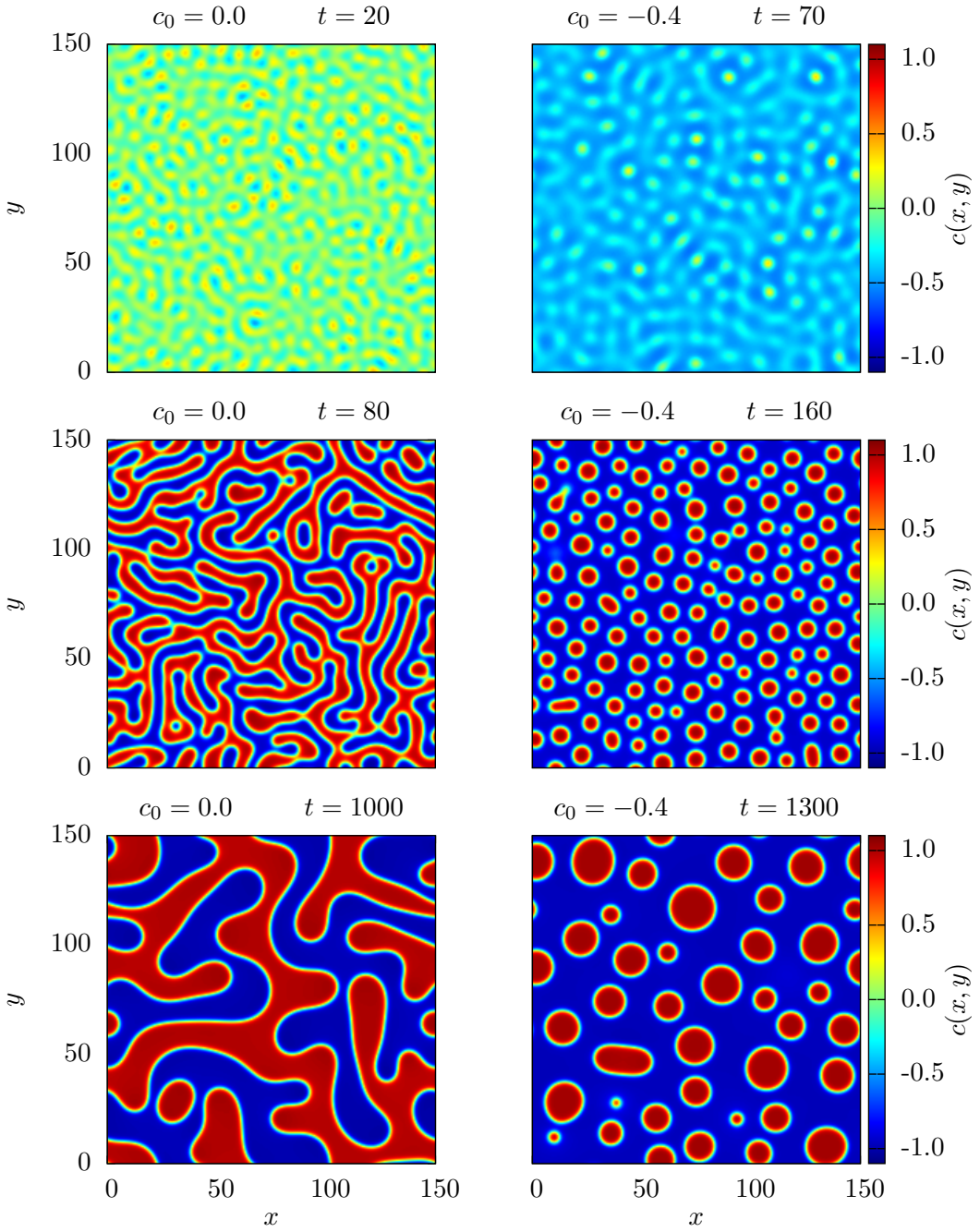

Figure 3.2.: Direct numerical simulations of the Cahn-Hilliard equation with the free energy density $f_0 = \frac{1}{4}(c^2 - 1)^2$ and $\kappa = 0.8$ showing phase separation into domains of $c_\mathrm{I} = -1.0$ and $c_\mathrm{II} = 1.0$. The two columns show the time evolution for the homogeneous and randomly perturbed initial condition $c_0 = 0.0$ and $c_0 = -0.4$. Note that the snapshots are not taken at equal times in the two columns. In both cases the coarsening dynamics are clearly exhibited. For the concentration $c_0 = -0.4$, which is closer to the binodal limit, one observes the formation of droplets. Smaller droplets are absorbed into larger ones, this process is known in literature as *Ostwald ripening* [Pis06].

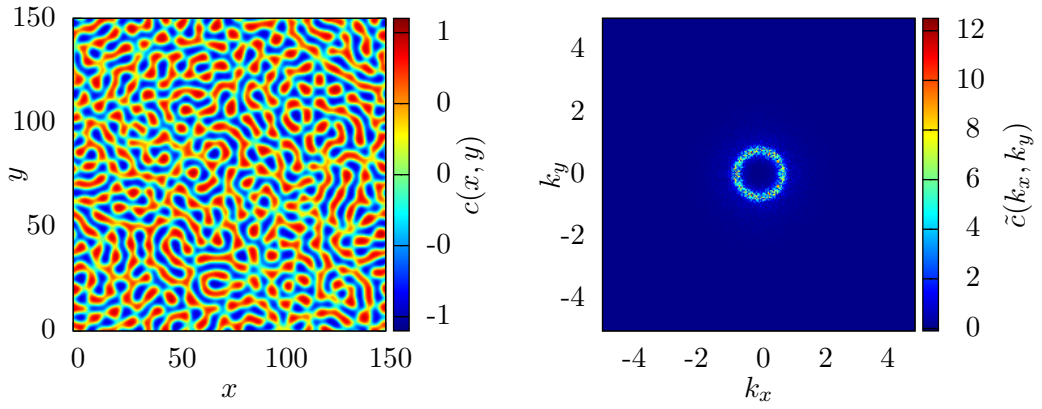

Figure 3.3.: Left: Snapshot of a 2D simulation of the classical Cahn-Hilliard equation at an early stage of the spinodal decomposition (t=30) for $c_0 = 0$ and $\kappa = 0.8$. Right: Discrete Fourier transformation of the simulation snapshot on the left. The value of the dominant mode corresponds well to the maximum of the corresponding dispersion relation (3.23).

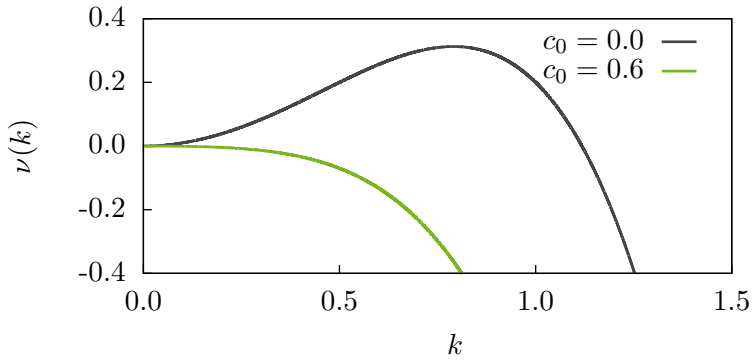

Figure 3.4.: Dispersion relations for the classical Cahn-Hilliard equation and two different homogeneous concentrations. The concentration $c_0 = 0.0$ lies in the spinodal region, the dispersion relation shows a finite band of unstable wavenumbers. The concentration $c_0 = 0.6$ lies in the binodal region but outside of the spinodal region. Here, the homogeneous solution is stable for all wavenumbers.

A second effect of the gradient contribution in the free energy is the so called *coarsening* of phase separated structures. As it can be clearly seen in figure 3.2, the dynamics are such that small domains of the same phase combine to larger domains in order to minimize the interface between the two phases and the corresponding energetic penalty. The numerical results and the dispersion relation shown in figures 3.2 -3.4 correspond to equation (3.12) with $M(c) = 1$ and the free energy density

$$f_0(c) = \frac{1}{4}(c^2 - 1)^2. \tag{3.24}$$

In the following, we will refer to this equation as the *classical* Cahn-Hilliard equation [CH58, NCS84].

3.4. Gradient Formulation of the Model Equations

The conservative part of the model equations derived in chapter 2 reads

$$\begin{aligned}
\partial_t h &= \boldsymbol{\nabla} \cdot \left(\frac{h^3}{3\eta(\phi)} \boldsymbol{\nabla} \left(\Pi(h) - \epsilon^3 \mathrm{Ca}^{-1} \Delta h \right) \right), \\
\partial_t \phi &= \left(\frac{h^2}{3\eta(\phi)} \boldsymbol{\nabla} \left(\Pi(h) - \epsilon^3 \mathrm{Ca}^{-1} \Delta h \right) \right) \cdot \boldsymbol{\nabla} \phi + \frac{1}{h} \left(\frac{1}{\mathrm{Pe}} (\boldsymbol{\nabla} (h D \boldsymbol{\nabla} \phi)) \right).
\end{aligned} \tag{3.25}$$

Note that in this section we adopt the notation (2.12), and therefore $\mathbf{x} \in \mathbb{R}^2$. In order to write these equations in a similar way as equation (3.12), i.e., as a gradient system, we start out by formulating a dimensional free energy functional for the thin solution layer depending on the height profile $h(\mathbf{x})$ and the local concentration $\phi(\mathbf{x})$. The formulation of equations (3.25) as a gradient system was first introduced by Thiele in [Thi11]. An appropriate choice is the following functional:

$$\mathcal{F}[h, \phi] = \int_A f(h) + \frac{\sigma}{2} (\nabla h)^2 + h \frac{k_\mathrm{B} T}{a^3} \phi \, \ln(\phi) \, dx^2. \tag{3.26}$$

Here $f(h)$ is the *disjoining potential*, representing the interaction energy between the solution and the substrate. The dimensional disjoining pressure $\Pi(h)$ is defined as $\Pi(h) = \frac{df}{dh}$. The second summand accounts for the surface energy of the film due to deformations and the third summand is the contribution of the concentration dependent bulk free energy.
One has to notice that in the set of equations (3.25) the fields which are conserved on the area A are not h and ϕ but rather h and $\Psi = h\phi$, since

$$\frac{d}{dt} \int_A dx^2 \, \Psi = \frac{d}{dt} \int_A h \, \frac{1}{h} \int_0^h dx^3 \, c\left(\mathbf{x}^{(\mathbf{3})} \right) = 0. \tag{3.27}$$

A gradient formulation of equations (3.25) is therefore only possible in terms of the fields $h(\mathbf{x})$ and $\Psi(\mathbf{x})$. We will show that a non-dimensional form of the following equations is equivalent to equations (3.25):

$$\begin{aligned}\partial_t h &= \nabla \cdot \left[Q_{hh} \nabla \frac{\delta F}{\delta h} + Q_{h\Psi} \nabla \frac{\delta F}{\delta \Psi} \right], \\ \partial_t \Psi &= \nabla \cdot \left[Q_{\Psi h} \nabla \frac{\delta F}{\delta h} + Q_{\Psi\Psi} \nabla \frac{\delta F}{\delta \Psi} \right],\end{aligned} \tag{3.28}$$

where the mobility matrix $\underline{\mathbf{Q}}$ is defined as

$$\underline{\mathbf{Q}} = \frac{1}{3\eta} \begin{pmatrix} h^3 & h^2\Psi \\ h^2\Psi & h\Psi^2 + \frac{3a^2}{6\pi}\Psi \end{pmatrix}. \tag{3.29}$$

Here, we also introduced the notation[2]:

$$F[\mathrm{h}, \Psi] := \mathcal{F}[h(\mathrm{h}, \Psi), \phi(\mathrm{h}, \Psi)], \tag{3.30}$$

with the nonlinear but bijective transformation

$$(h, \phi) \leftrightarrow (\mathrm{h}, \Psi), \text{where } h(\mathrm{h}, \Psi) = \mathrm{h}; \quad \phi(\mathrm{h}, \Psi) = \frac{\Psi}{\mathrm{h}}. \tag{3.31}$$

Equations (3.28) can be rescaled using the scaling introduced in (2.13) and a scaling for the energy $F = e_0 l_0^2 \tilde{F}$ (here e_0 is an energy per area). Since we interpret the concentration as a per volume concentration, the quantity $\Psi = h\phi$ can be seen as a local height of the solute and is scaled according to $\Psi = h_0 \tilde{\Psi}$. We scale the molecular length by the small length scale h_0. The scaling of the mobility matrix therefore reads $\underline{\mathbf{Q}} = \frac{h_0^3}{\eta_0} \underline{\tilde{\mathbf{Q}}}$. Furthermore, it is important to note the following correspondence between rescaling and functional derivatives[3]:

$$\frac{\delta}{\delta h(\mathbf{x})} \rightarrow \frac{1}{l_0^2 h_0} \frac{\delta}{\delta \tilde{h}(\tilde{\mathbf{x}})}. \tag{3.32}$$

We rescale equation (3.28) and immediately drop the tildes as usual:

$$\begin{aligned}\frac{\eta_0 h_0}{t_0 \epsilon^2 e_0} \partial_t h &= \nabla \cdot \left[\frac{h^3}{3\eta} \nabla \frac{\delta F}{\delta h} + \frac{h^2\Psi}{3\eta} \nabla \frac{\delta F}{\delta \Psi} \right], \\ \frac{\eta_0 h_0}{t_0 \epsilon^2 e_0} \partial_t \Psi &= \nabla \cdot \left[\frac{h^2\Psi}{3\eta} \nabla \frac{\delta F}{\delta h} + \left(\frac{h\Psi^2}{3\eta} + \frac{a^2}{6\pi\eta h_0^2} \Psi \right) \nabla \frac{\delta F}{\delta \Psi} \right].\end{aligned} \tag{3.33}$$

[2] In this section and in the following, we often omit the differentiation between h and h, since the differentiation between $\mathcal{F}$ and F always clarifies in a unique way which field we mean.

[3] The initial functional derivative acts on a functional of the type $F = \int_A ...dx^2$, whereas the rescaled functional derivative acts on a functional of the type $\tilde{F} = \int_{\tilde{A}} ...d\tilde{x}^2$, hence the factor $1/l_0^2 = \left(\frac{\tilde{x}}{x}\right)^2$.

The effective time scale $\frac{t_0\epsilon^2 e_0}{\eta_0 h_0}$ is now defined to be unity, and we thus establish the relationship

$$t_0 = \frac{\eta_0 h_0}{\epsilon^2 e_0} \tag{3.34}$$

between energy and time scale of the equations, which was already used in the scaling of the pressure term in the derivation of the basic equations (see chapter 2, section 2.2). The non-dimensional free energy functional reads:

$$F[h,\Psi] = \int \frac{\sigma\epsilon^2}{2e_0}(\nabla h)^2 + \frac{1}{e_0} f(h_0 h) + h\frac{h_0 k_\mathrm{B} T}{a^3 e_0}\frac{\Psi}{h}\,\ln\left(\frac{\Psi}{h}\right) dA. \tag{3.35}$$

For calculations, it is convenient to perform the transformation (3.31) and to reformulate equations (3.33) in terms of $(\mathcal{F}, h, \phi)$, so that variations with respect to h and ϕ are performed independently. We use the relations

$$\begin{aligned}\frac{\delta F[h,\Psi]}{\delta h} &= \frac{\delta \mathcal{F}[\mathrm{h}(h,\Psi),\phi(h,\Psi)]}{\delta h} = \frac{\partial \phi}{\partial h}\frac{\delta \mathcal{F}[\mathrm{h},\phi]}{\delta \phi} + \frac{\partial \mathrm{h}}{\partial h}\frac{\delta \mathcal{F}[\mathrm{h},\phi]}{\delta \mathrm{h}} \\ &= \frac{\delta \mathcal{F}[\mathrm{h},\phi]}{\delta \mathrm{h}} - \frac{\phi}{\mathrm{h}}\frac{\delta \mathcal{F}}{\delta \phi}, \end{aligned} \tag{3.36}$$

$$\frac{\delta F[h,\Psi]}{\delta \Psi} = \frac{\partial \phi}{\partial \Psi}\frac{\delta \mathcal{F}[\mathrm{h},\phi]}{\delta \phi} + \frac{\partial \mathrm{h}}{\partial \Psi}\frac{\delta \mathcal{F}[\mathrm{h},\phi]}{\delta \mathrm{h}} = \frac{1}{\mathrm{h}}\frac{\delta \mathcal{F}}{\delta \phi}. \tag{3.37}$$

and obtain

$$\partial_t h = \nabla\cdot\left(Q_{hh}\left(\nabla\frac{\delta\mathcal{F}}{\delta h} - \frac{1}{h}\frac{\delta\mathcal{F}}{\delta\phi}\nabla\phi\right)\right) \tag{3.38}$$

$$\partial_t \phi = \frac{Q_{hh}}{h}\left(\nabla\frac{\delta\mathcal{F}}{\delta h} - \frac{1}{h}\frac{\delta\mathcal{F}}{\delta\phi}\nabla\phi\right)\cdot\nabla\phi + \frac{1}{h}\nabla\cdot\left(Q_{\mathrm{diff}}\nabla\left(\frac{1}{h}\frac{\delta F}{\delta\phi}\right)\right). \tag{3.39}$$

By $\mathcal{F}$ we mean the (h,ϕ) dependent analog to the non-dimensional functional (3.35) and we have defined $Q_{\mathrm{diff}} := \frac{h\phi a^2}{6\pi h_0^2 \eta}$. The variations read

$$\frac{\delta\mathcal{F}}{\delta h} = -\frac{\sigma\epsilon^2}{e_0}\Delta h + \frac{h_0}{e_0}f'(h_0 h) + \frac{h_0 k_\mathrm{B} T}{a^3 e_0}\phi\,\ln(\phi)\,; \quad \frac{\delta\mathcal{F}}{\delta\phi} = \frac{h_0 k_\mathrm{B} T}{a^3 e_0} h\,(\ln(\phi)+1)\,. \tag{3.40}$$

By inserting these variations into equation (3.33), we finally recover equations (3.25), since, due to (3.34),

$$\frac{\sigma\epsilon^2}{e_0} = \frac{t_0\epsilon\sigma}{\eta_0 h_0}\epsilon^3 = Ca^{-1}\epsilon^3, \tag{3.41}$$

$$\frac{3a^2}{6\pi h_0^2}\frac{h_0 k_\mathrm{B} T}{a^3 e_0} = \frac{k_\mathrm{B} T}{6\pi a}\frac{1}{e_0 h_0} = \frac{k_\mathrm{B} T}{6\pi a \eta_0}\frac{t_0\epsilon^2}{h_0^2} = \frac{1}{Pe}. \tag{3.42}$$

The nondimensional disjoining pressure is defined as $\Pi(h) = \frac{h_0}{e_0} f'(h_0 h)$. We will now adopt a special choice of scales, which will prove itself useful later on. We choose

$$e_0 := \frac{E_0}{h_0^2}; \quad l_0 = h_0^2 \sqrt{\frac{\sigma}{E_0}}, \tag{3.43}$$

where E_0 is an arbitrary energy scale. The choice of the lengthscale l_0 implies $\frac{\sigma \epsilon^2}{e_0} = 1$. By defining the dimensionless parameters

$$L := \frac{h_0}{a}; \quad E_T = \frac{k_\mathrm{B} T}{E_0}, \tag{3.44}$$

we can finally write the rescaled free energy as

$$\mathcal{F}[h, \phi] = \int \frac{1}{2} (\nabla h)^2 + \frac{h_0^2}{E_0} f(h_0 h) + h L^3 E_T \ \phi \ \ln(\phi) \, dA. \tag{3.45}$$

The parameter L is obviously the ratio of a typical film height to the molecular length scale a and E_T is the ratio of the thermal energy $k_\mathrm{B} T$ and the reference energy scale E_0 which is yet to be chosen.
We briefly return to the discussion of the general structure of equation (3.28). The mobility matrix $\underline{\mathbf{Q}}$ has two important properties. Firstly, the matrix is positive definite, a fact which ensures the Lyapunov functional property of F in equations (3.28):

$$\begin{aligned} \frac{d}{dt} F &= \int_A \frac{\delta F}{\delta h(\mathbf{x}')} \partial_t h(\mathbf{x}', t) + \frac{\delta F}{\delta \Psi(\mathbf{x}')} \partial_t \Psi(\mathbf{x}', t) \ dx'^2 \\ &= - \int_A \begin{pmatrix} \nabla \frac{\delta F}{\delta h} \\ \nabla \frac{\delta F}{\delta \Psi} \end{pmatrix}^T \underline{\mathbf{Q}} \begin{pmatrix} \nabla \frac{\delta F}{\delta h} \\ \nabla \frac{\delta F}{\delta \Psi} \end{pmatrix} \ dx'^2 < 0. \end{aligned} \tag{3.46}$$

Secondly the matrix $\underline{\mathbf{Q}}$ is symmetric. Due to this fact, the formulation (3.28), can be interpreted in close relation to the so called *Onsager reciprocity relation* [GP71], where $\mathbf{F}_h = \nabla \frac{\delta F}{\delta h}$, $\mathbf{F}_\Psi = \nabla \frac{\delta F}{\delta \Psi}$ are the thermodynamic forces corresponding to irreversible processes.
As already emphasized in the former chapter, equations (3.25) are valid only for small concentrations, where the dynamics are purely diffusional. Using the gradient formulation, we are now in the position to extend equations (3.25) in a consistent way, i.e., such that the gradient structure remains unaltered. In the following section we will derive a bulk free energy $f_B(c, \nabla c)$ which is valid for high concentrations and local interactions in the solution. We will then replace the purely entropic bulk free energy $\overline{g}(\phi) = \frac{k_\mathrm{B} T}{a^3} \phi \ln(\phi)$ in (3.26) by $f_B(\phi, \nabla \phi)$.

3.5. Free Energy of a Non-Ideal Solution

In this section, we provide a derivation of the free energy density of a solution with locally interacting components (known in literature as a *regular solution* [Gug35]) in the framework of classical statistical mechanics. The derivation follows closely the arguments presented in [Saf94] (chapter 2, section 3).
We assume that the solvent and solute have a similar hard-core repulsion radius and the solution can thus be modeled by a lattice Hamiltonian with a single lattice constant a corresponding to the molecular length of the components. The lattice sites representing spatial coordinates $\mathbf{r}_i$, $\mathbf{r}_j$ will be denoted by indices i and j, respectively. The Hamiltonian of the system reads:

$$\mathcal{H} = -\frac{1}{2}\sum_{i,j} J_{ij}^{AA}(1-s_i)(1-s_j) + J_{ij}^{BB}s_i s_j + 2J_{i,j}^{AB}s_i\,(1-s_j)\,. \tag{3.47}$$

Here, the quantities $J_{ij}^{AA}, J_{ij}^{BB}, J_{ij}^{AB}$ are positive energies of attractive solvent-solvent (AA), solute-solute (BB) and solvent-solute (AB) interactions. Furthermore we define $s_i \in \{0,1\}$, so that $s_i = 0$ if the lattice site i is occupied by a solvent molecule, and $s_i = 1$ if the site is occupied by a solute molecule:

$$\mathcal{H}_{\text{int}} = \frac{1}{2}\sum_{i,j} J_{ij} si(1-s_j), \quad \text{where} \;\; J_{ij} = \frac{1}{2}\sum_{ij}(J_{ij}^{AA} + J_{ij}^{BB} - 2J_{ij}^{AB}). \tag{3.48}$$

$\mathcal{H}_{\text{int}}$ is the effective interaction Hamiltonian, which can be derived from $\mathcal{H}$ by neglecting constant terms. The effective interaction energy between solute and solvent J_{ij} is positive and thus repulsive, if the interaction energies of molecules of the same type are greater then J_{ij}^{AB}. We now calculate an upper bound to the free energy corresponding to the Hamiltonian $\mathcal{H}_{\text{int}}$. For this purpose, we define a model (or trial) Hamiltonian by

$$\mathcal{H}_0 = \sum_i k_{\text{B}}T\alpha_i s_i. \tag{3.49}$$

The interaction energies $k_{\text{B}}T\alpha_i$ are now merely locally defined and, as we will show, dependent on a quantity we define as the local concentration. The model Hamiltonian defines a model probability weight $P_0(s_i)$ and configuration sum Z_0 as well as a model equilibrium free energy F_0:

$$Z_0 = \sum_{\{s_i\}\in\{0,1\}^N} e^{-\frac{\mathcal{H}_0(\{s_i\})}{k_{\text{B}}T}} = \sum_{\{s_i\}\in\{0,1\}^N} e^{\sum_i -\alpha_i s_i} = \prod_i \sum_{s_i=0,1} e^{-\alpha_i s_i} = \prod_i \frac{1}{1-\phi_i}. \tag{3.50}$$

$$P_0(\{s_i\}) = \frac{e^{-\frac{\mathcal{H}_0(\{s_i\})}{k_{\text{B}}T}}}{Z_0}; \quad F_0 = -k_{\text{B}}T\,\ln(Z_0) = k_{\text{B}}T\sum_i \ln(1-\phi_i). \tag{3.51}$$

We have introduced the quantity $\phi := (1+e^{\alpha_i})^{-1}$. It is readily shown that

$$\phi_i = \langle s_i\rangle_0, \tag{3.52}$$

where by $\langle \dots \rangle_0$, we mean the statistical average with respect to the statistical weight P_0 defined above. Equation (3.52) states that ϕ_i corresponds to the local mean value of s_i with respect to the model Hamiltonian and since $s_i \in \{0, 1\}$ we identify ϕ_i as the local concentration of the solute. One can furthermore derive the following inequality which holds for all parameters $\{\alpha_i\}$:

$$F_{\text{exact}} < F_0 + \langle \mathcal{H}_{\text{int}} - \mathcal{H}_0 \rangle_0 =: F. \tag{3.53}$$

Assuming that H_0 allows a good approximation of the full Hamiltonian, the minimum of $F(\phi_i)$ with respect to the local concentrations ϕ_i provides an upper bound close to the equilibrium free energy of the full system. Close to equilibrium, F is then a good approximation for the free energy of the non-homogeneous system. Inserting relations (3.50),(3.50) into the definition (3.53) yields:

$$\begin{aligned} F &= k_{\text{B}}T \sum_i (1-\phi_i)\ln(1-\phi_i) + \phi_i \ln(\phi_i) + \frac{1}{2}\sum_{i,j} J_{ij}\phi_i(1-\phi_j) \qquad (3.54)\\ &= k_{\text{B}}T \sum_i (1-\phi_i)\ln(1-\phi_i) + \phi_i \ln(\phi_i) + \frac{1}{2}\sum_{i,j} \frac{1}{2} J_{ij}\left((\phi_i-\phi_j)^2 - \phi_i^2 - \phi_j^2 + 2\phi_i\right). \end{aligned}$$

In the continuum limit and for local (nearest neighbor) interactions, the free energy can finally be written as:

$$F[c] = \int_V dx^3 f_B(c, \nabla c), \tag{3.55}$$

$$\begin{aligned} \text{where} \quad f_B(c,\nabla c) &= \frac{k_{\text{B}}T}{a^3}\left(c\,\ln(c) + (1-c)\,\ln(1-c)\right) + \frac{J}{a^3}\,c(1-c) + \frac{1}{2}\frac{J}{a}(\nabla c)^2 \\ &=: g(c) + \frac{1}{2}\frac{J}{a}(\nabla c)^2. \end{aligned} \tag{3.56}$$

Note that the free energy $g(c)$ corresponds in fact to a special case of the well known *Flory-Huggins* free energy for polymer solutions, which reads [deG79]

$$g_{\text{FH}} = \frac{c}{N}\,\ln(c) + (1-c)\,\ln(1-c) + \chi\, c(1-c), \tag{3.57}$$

where χ is an interaction parameter and N is the number of monomers of which the considered polymer is constituted.

3.6. Extended Equations

As already stated, to extend our basic equations (3.25) we will now insert the bulk free energy density derived above as a replacement of the bulk free energy density of purely entropic type. This ansatz is based on the important assumption that the mobility

matrix remains unaltered for higher concentrations and interacting molecules. The extended overall free energy functional of the thin film now reads

$$\mathcal{F}[h,\phi] = \int \frac{1}{2}(\nabla h)^2 + \frac{h_0^2}{E_0} f(h_0 h) + h f_B(\phi, \nabla\phi)\ dx^2, \tag{3.58}$$

where $f_B(\phi, \nabla\phi)/h_0$ is given by a rescaled version of (3.56):

$$f_B(\phi, \nabla\phi) = g(\phi) + \epsilon^2 E_J L \frac{1}{2}(\nabla\phi)^2, \tag{3.59}$$

$$g(\phi) = L^3 E_T\,(\phi\ \ln(\phi) + (1-\phi)\ \ln(1-\phi)) + L^3 E_J \phi(1-\phi). \tag{3.60}$$

In analogy to the parameter E_T, we defined the dimensionless quantity $E_J = \frac{J}{E_0}$ as the ratio of the bulk interaction energy J and the reference energy scale E_0. For convenience we furthermore define

$$\alpha := \frac{E_J}{E_T}\left(= \frac{J}{k_B T}\right); \quad \gamma := \epsilon^2 E_J L. \tag{3.61}$$

The variations with respect to (h, ϕ) are now given by

$$\frac{\delta\mathcal{F}}{\delta h} = g(\phi) + \frac{\gamma}{2}(\nabla\phi)^2 - \Delta h + f'(h), \tag{3.62}$$

$$\frac{\delta\mathcal{F}}{\delta\phi} = h g'(\phi) - \gamma\nabla(h\nabla\phi). \tag{3.63}$$

These variations can be inserted in equations (3.39) and we obtain the following extended equations:

$$\partial_t h = \nabla\cdot\left(Q_{hh}\left(\nabla\left(-\Delta h + f'(h) + \frac{\gamma}{2}(\nabla\phi)^2\right) + \frac{\gamma}{h}\nabla\cdot(h\nabla\phi)\nabla\phi\right)\right), \tag{3.64}$$

$$\begin{aligned}\partial_t\phi =& \frac{Q_{hh}}{h}\left(\nabla\left(-\Delta h + f'(h) + \frac{\gamma}{2}(\nabla\phi)^2\right) + \frac{\gamma}{h}\nabla\cdot(h\nabla\phi)\nabla\phi\right)\cdot\nabla\phi + \\ & \frac{1}{h}\nabla\left(\frac{h\phi}{6\pi L^2\eta}\nabla\left(g'(\phi) - \frac{1}{h}\gamma\nabla(h\nabla\phi)\right)\right).\end{aligned} \tag{3.65}$$

We note two important aspects of the extended equations. Firstly, as it could have been expected, the effective (linear) diffusion coefficient in the diffusive contribution to the time evolution of ϕ is changed according to the non-gradient part $g(\phi)$ of the bulk free energy. The equation for ϕ is also supplemented by a term containing derivatives of higher order and especially a negative biharmonic term in ϕ. The consequences of these extensions will be discussed in detail in the next chapter.

Secondly, the hydrodynamic flux $\mathbf{J}_{\text{adv}}$ corresponding to the flux in equation (3.64) is now dependent on gradients in the concentration field ϕ. These terms stem from a concentration-dependent *Cauchy stress tensor* which has to be inserted in the Navier-Stokes equation for the case of interacting solute molecules [LT98].
The extended equations for a general bulk free energy density are still of the form

$$\partial_t \phi = -\frac{1}{h}\mathbf{J}_{\text{adv}} \cdot \boldsymbol{\nabla}\phi + \frac{1}{h}\nabla \cdot \left(Q_{\text{diff}} \nabla \left(\frac{1}{h}\frac{\delta F_B}{\delta \phi} \right) \right). \tag{3.66}$$

The term $\frac{1}{h}\mathbf{J}_{\text{adv}}$ corresponds to the height averaged velocity of the solution. In [NT10], the authors were able to derive this term rigorously from a generalized Navier-Stokes equation in the framework of a thin film limit of the Navier-Stokes Cahn-Hilliard (NSCH) equations. For the case of concentration independent disjoining potential and surface tension, the free energy functional F_B simply reads

$$F_B = \int\limits_A h\ f_B(\phi, \nabla\phi)\ dx^2. \tag{3.67}$$

We now propose a derivation for the general form of the diffusive contribution in analogy to the derivation presented in 2.2.2. We start with a generalized diffusion equation of Cahn-Hilliard type, valid in the volume $V = \int\limits_A h(\mathbf{x})dx^2$ of the film:

$$\partial_t c\left(\mathbf{x}^{(\mathbf{3})}, t\right) = \nabla^{(\mathbf{3})} \cdot \left(M(c)\nabla^{(\mathbf{3})} \frac{\delta F_V[c]}{\delta c} \right). \tag{3.68}$$

The free energy functional F_V is defined as a volume integral over an arbitrary free energy density:

$$F_V = \int f(c, \nabla^{(\mathbf{3})} c) dx^3. \tag{3.69}$$

We now introduce general scales (J_0, J_0^z) for the flux $\mathbf{J} := -\left(M(c)\nabla^{(\mathbf{3})} \frac{\delta F_V[c]}{\delta c} \right)$ in the horizontal plane and the vertical flux $J^z := -\left(M(c)\partial_z \frac{\delta F_V[c]}{\delta c} \right)$ respectively. As in 2.2.2, we then average the equation over the film height and obtain

$$\partial_t \phi(\mathbf{x}, t) + \epsilon^2 \frac{1}{h} \int\limits_0^{h(\mathbf{x},t)} \partial_t c_1(\mathbf{x}, z, t)\ dz = -\frac{J_0 t_0}{l_0}\frac{1}{h} \int\limits_0^{h(\mathbf{x},t)} \nabla \cdot \mathbf{J} dz - \frac{J_0^z t_0}{h_0}\frac{1}{h}(J^z|_{z=h} - J^z|_{z=0}). \tag{3.70}$$

We performed the ansatz $c(\mathbf{x}, z, t) = \phi(\mathbf{x}, t) + \epsilon^2 c_1(\mathbf{x}, z, t)$. The choice of the parameter of smallness of the z dependent summand is of no importance for the derivation

presented. For the purely diffusional case, the no flux boundary condition at the free surface reads:

$$\frac{J_0^z t_0}{h_0} J^z|_{z=h} = \frac{J_0 t_0}{l_0} \mathbf{J}|_{z=h} \cdot \nabla h. \tag{3.71}$$

Using this boundary condition, as well as the no flux boundary condition at the substrate, equation (3.70) is reformulated as

$$\partial_t \phi(\mathbf{x},t) + \epsilon^2 \frac{1}{h} \int_0^{h(\mathbf{x},t)} \partial_t c_1(\mathbf{x},z,t)\, dz = -\frac{J_0 t_0}{l_0} \frac{1}{h} \nabla \cdot \int_0^{h(\mathbf{x},t)} \mathbf{J} dz. \tag{3.72}$$

A functional Taylor expansion of the free energy F_V yields the straight forward result

$$\begin{aligned} F_V[c] &= F_V[\phi] + \epsilon^2 \int_V \left. \frac{\delta F[c]}{\delta c(\mathbf{x}',z',t)} \right|_{c(\mathbf{x}',z',t)=\phi(\mathbf{x}',t)} c_1(\mathbf{x}',z',t)\, dx'^3 \\ &= F_V[\phi] + \mathcal{O}(\epsilon^2). \end{aligned} \tag{3.73}$$

Omitting all terms of order $\mathcal{O}(\epsilon^2)$ or higher order in ϵ, we now obtain:

$$\partial_t \phi(\mathbf{x},t) = \frac{J_0 t_0}{l_0} \frac{1}{h} \nabla \cdot \left(h M(\phi) \nabla \frac{\delta F_B[\phi]}{\delta c(\mathbf{x},z,t)} \right), \tag{3.74}$$

where F_B is given by $F_B[\phi] = \int_V f(\phi, \nabla\phi)\, dx^3 = \int_A h\, f(\phi, \nabla\phi)\, dx^2$ as in equation (3.67). Since $\phi[c(\mathbf{x})] = \frac{1}{h} \int_0^h c(\mathbf{x},z')dz'$, we finally observe that[4]

$$\begin{aligned} \frac{\delta F_B[\phi]}{\delta c(\mathbf{x},z,t)} &= \frac{\delta F_B[\phi[c]]}{\delta c(\mathbf{x},z,t)} = \int_A \frac{\delta F_B[\phi]}{\delta \phi(\mathbf{x}',t)} \frac{\delta \phi[c(\mathbf{x}')]}{\delta c(\mathbf{x},z,t)} dx'^2 \\ &= \int_A \frac{\delta F_B[\phi]}{\delta \phi(\mathbf{x}',t)} \frac{1}{h(\mathbf{x}')} \int_0^{h(\mathbf{x}',t)} \delta(\mathbf{x}-\mathbf{x}')\delta(z''-z')dz''dx'^2 = \frac{1}{h(\mathbf{x},t)} \frac{\delta F_B[\phi]}{\delta \phi(\mathbf{x},t)} \end{aligned} \tag{3.75}$$

Equation (3.74) then reads

$$\partial_t \phi(\mathbf{x},t) = \frac{J_0 t_0}{l_0} \frac{1}{h} \nabla \cdot \left(h M(\phi) \nabla \frac{1}{h(\mathbf{x},t)} \frac{\delta F_B[\phi]}{\delta \phi(\mathbf{x},t)} \right), \tag{3.76}$$

which is in agreement with (3.66) for $M(c) \propto c/\eta(c)$. We have thus shown that the extension of the bulk free energy in equations (3.25) leads to a modified diffusional part,

[4] As it is often the case for the variational calculus in theoretical physics, we lack in mathematical rigour in our derivation. For the special free energy functionals we are interested in, the identity (3.75) can be justified through a detailed but simple calculation. The admittedly ill defined chain rule used here is proposed in [GR93].

which can be derived starting from a Cahn-Hilliard type equation for the non-averaged concentration. The special type of extension we will use in the following (i.e. the bulk free energy density for a regular solution) is a straight forward extension of the purely entropic free energy which gives rise to the simple diffusion equation, as shown in (3.8). The mobility coefficient $M(c) \propto c/\eta(c)$ is chosen such that for small concentrations (where $\eta(c) \approx \eta$) and non-interacting particles the diffusion equation is recovered. For concentration independent viscosities, an alternative choice yielding a diffusion equation for the quantity $(1-c)$ for high concentrations would be $M(c) \propto c(1-c)$. However, for concentration dependent viscosities, this mobility supplemented by $1/\eta$ does not lead to a linear diffusion equation in $(1-c)$ and is not considered in this work.

4. Thin Solution Layers on a Resting Substrate

In this chapter, we discuss the stability and dynamics of thin solution layers on a substrate which is at rest. We will first consider a thin layer of a simple fluid, i.e., the case $\phi = 0$, and introduce two alternative formulations of the disjoining potential term. For the case $\phi \neq 0$, we will then complement the extended equations (3.64) by an expression for the evaporation and the concentration-dependent viscosity, and discuss the linear stability of the resulting equations as well as phase separation and dewetting, including nonlinear effects.

4.1. The Thin Film Equations for Simple Liquids

For the case of a pure liquid, i.e., for $\phi(\mathbf{x}) = 0$, equations (3.64) reduce to the extensively investigated thin film equation (e.g., [KT07])

$$\partial_t h = \nabla \cdot \left[Q_{hh} \nabla \frac{\delta F_{\mathrm{SF}}[h]}{\delta h} \right] = \nabla \cdot \left[Q_{hh} \nabla \left(-\Delta h + \frac{h_0^3}{E_0} f'(h_0 h) \right) \right] \tag{4.1}$$

This equation, although not derived from the point of view of phase separation, is of Cahn-Hilliard type with a nonlinear mobility Q_{hh} and a free energy functional

$$F_{\mathrm{SF}}[h] = \int \left(\frac{1}{2} (\nabla h)^2 + \frac{h_0^2}{E_0} f(h_0 h) \right) \, dx^2, \tag{4.2}$$

where a rescaled version of the disjoining potential corresponds to the local free energy f_0 in (3.12). The disjoining potential therefore determines the linear stability of homogeneous solutions of equation (4.1). Before discussing suitable choices of the disjoining potential, we need to establish some physical background concerning thin liquid films on substrates.

Depending on the interaction energy of the liquid with the surface of the substrate, three scenarios, well known from daily experiences, may occur when a liquid is deposited on a substrate. As shown in figure 4.1, depending on the *equilibrium contact angle*, which is determined by *Young's equation* [Saf94], in equilibrium, the substrate is partially, completely or not at all covered. For the partially wetting case, a homogeneous film will eventually break up to form droplets, whose shape is determined by the amount of mass and the contact angle.

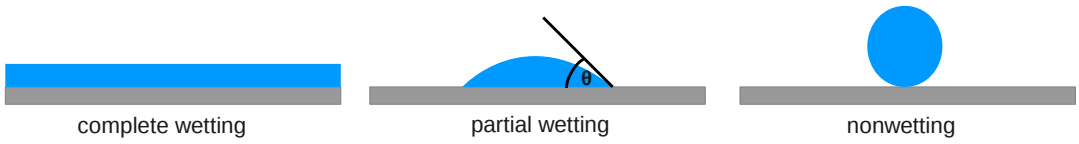

Figure 4.1.: Sketch of the three different wetting scenarios for thin films deposited on a substrate. The contact angle θ is determined by the substrate-liquid interaction and the surface tension of the film through Young's equation [Saf94].

The mathematical description of thin films in terms of a continuum model becomes quite delicate whenever applied to a three phase boundary (*trijunction*), like in the case of a contact line of a film or droplet. If the contact line moves on the substrate (e.g., when the substrate is pulled out of a liquid bath), the velocity of the fluid in terms of the hydrodynamic continuum theory is multivalued due to the no-slip boundary condition which is in general applied in fluid mechanics. The stress then diverges logarithmically at the contact line [BMW02]. The moving contact line problem was first pointed out rigorously in [HS71] and has since then become a field of research of its own, which is out of the scope of this thesis. A quite simple approach to circumvent the problem is to introduce the concept of a so called *precursor film*. According to this approach, at the henceforth merely apparent contact line, the film fades into the ultrathin precursor (see figure 4.2). The contact line problem is transferred to the trijunction of the precursor film which is simply not described. For the description of partially wetted surfaces, one therefore assumes that the "dry" regions are completely covered by the precursor film.

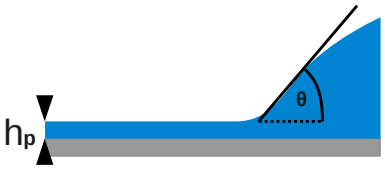

Figure 4.2.: Sketch of a contact line placed on an ultrathin precursor h_{p} and of the apparent contact angle θ.

In order to include the concept of a precursor film in the framework of our thin film equations, we obviously need to formulate a disjoining potential which provides (for the case of dewetting) a stable fixed point of homogeneous film height h_p corresponding to the height of the precursor. The disjoining pressure $\Pi(h)$ was experimentally found and described by Derjaguin [Der40]. It becomes relevant for films of thickness smaller than 100 nm, since apolar *van der Waals* forces extend across the whole thickness of the film in those geometries [BMW02].

In this work, we will use two different models for the disjoining potential $f(h)$, namely

$$f_{\mathrm{P}}(h) = -\frac{A}{2h^2} + \frac{B}{5h^5}, \tag{4.3}$$

$$f_{\mathrm{S}}(h) = \frac{A}{2h^2} + S^{\mathrm{P}} e^{\frac{d_0-h}{\delta_0}}. \tag{4.4}$$

The disjoining potential f_{P} was derived by Pismen [Pis01] in the framework of a diffuse interface model for thin apolar films. The first term in f_{P} stems from long-range van der Waals interactions. The constant typically characterizing van der Waals interactions is the *Hamaker constant* A_{H} [Isr11], and for f_{P} the relation $A = -\frac{A_{\mathrm{H}}}{6\pi}$ holds. The second summand in f_{P} corresponds to a short-range repulsive term with some constant B. The potential f_{S} was proposed by Sharma for polar fluids [Sha93] . Here, the constant A is the same as for the potential f_{P}, $S^{\mathrm{P}} < 0$ is a polar spreading coefficent, d_0 and δ_0 are the *Born repulsion length* and the *Debye length*, respectively [TVA$^+$09]. In the scaling of our basic equations, we are still free to choose the length scale h_0 and the energy scale E_0. These scales are now chosen such that the coefficients in the disjoining pressures are eliminated. We define

$$h_0 := \sqrt[3]{\frac{B}{A}}; \qquad E_0 = A \qquad \text{for} \qquad f(h) = f_{\mathrm{P}}(h), \tag{4.5}$$

$$h_0 := \sqrt[3]{\frac{\delta_0 A e^{-\frac{d_0}{\delta_0}}}{|S^{\mathrm{P}}|}}; \qquad E_0 = A \qquad \text{for} \qquad f(h) = f_{\mathrm{S}}(h). \tag{4.6}$$

The non-dimensional potentials then read

$$\frac{h_0^2}{E_0} f_{\mathrm{P}}(h_0 h) = -\frac{1}{2h^2} + \frac{1}{5h^5}; \qquad \frac{h_0^2}{E_0} f_{\mathrm{S}}(h_0 h) = \frac{1}{2h^2} - \frac{1}{\chi} e^{-\chi h}, \tag{4.7}$$

where we defined $\chi := h_0/\delta_0$. In the following, we will refer to the nondimensional disjoining potentials (4.7) simply as $f_{\mathrm{P,S}}(h)$. The two potentials and the corresponding pressures are plotted in figure (4.3).
Since, as already mentioned, equation (4.1) is of Cahn-Hilliard type, the linear stability of homogeneous films of height h_0 is determined by a dispersion relation of the same form as (3.23):

$$\nu(k) = Q_{hh}(h_0) \left(- \left. \frac{\partial^2 f_{\mathrm{P,S}}}{\partial h^2} \right|_{h=h_0} k^2 - k^4 \right). \tag{4.8}$$

The limits of the stable region (spinodal lines) are given by $\left. \frac{\partial^2 f_{\mathrm{P,S}}}{\partial h} \right|_{h=h_0} = 0$ and are also shown in figure (4.3). Outside of the linear stable region, homogeneous films break-up into "dry" regions (i.e. regions with $h = h_{\mathrm{p}}$) and regions of larger film heights. This process in the context of the thin film equation (4.1) is called *spinodal dewetting*, in

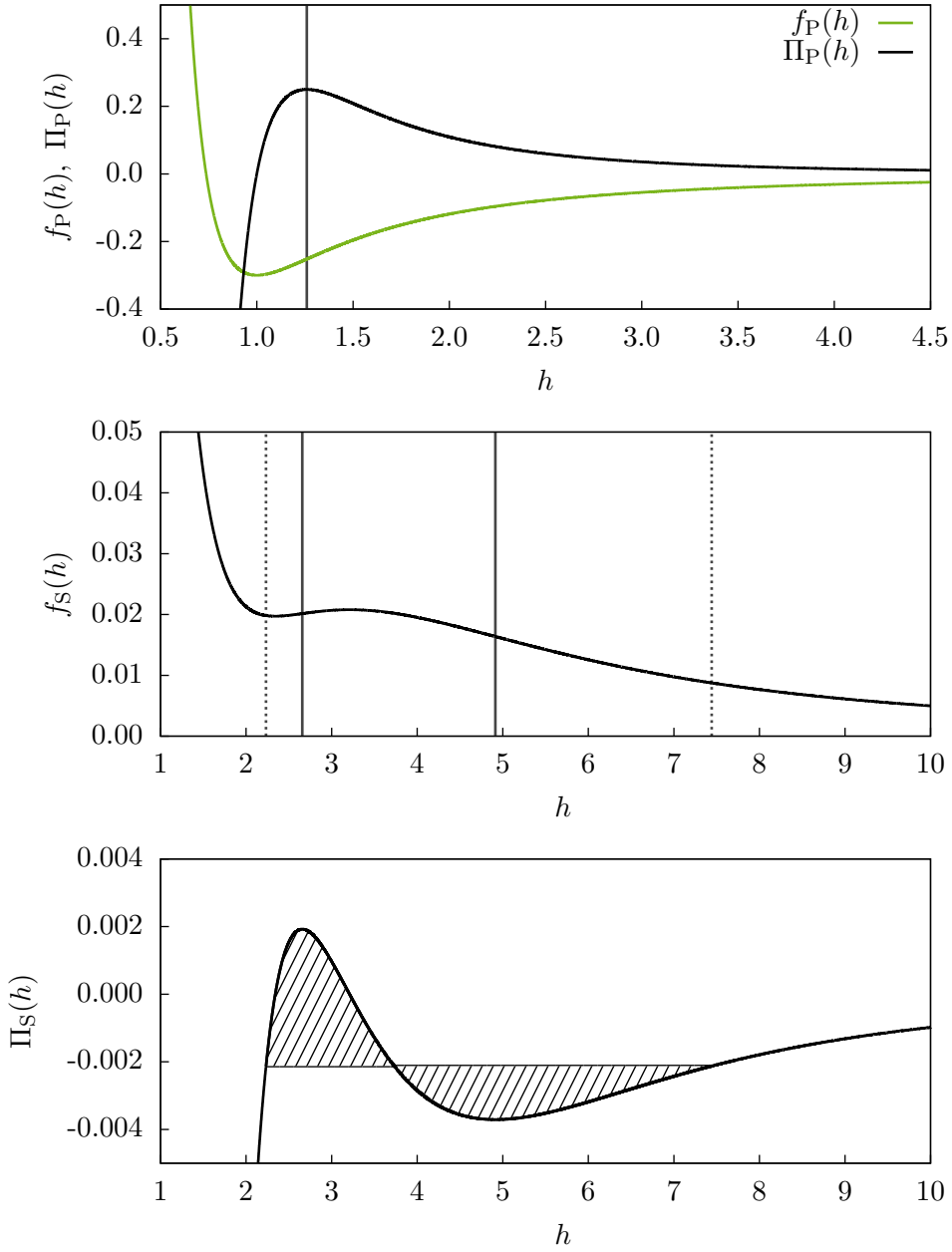

Figure 4.3.: Plots of the disjoining potentials f_P, f_s, given by (4.3), (4.4) and of the corresponding disjoining pressures Π_P, Π_S. The solid lines designate the spinodal region, which extends to infinity for f_P. For f_S, one finds two coexisting film heights which define the limits of the binodal region, as denoted by the dotted lines. The corresponding Maxwell construction is shown in the plot of Π_S.

analogy to the spinodal decomposition in the classical Cahn-Hilliard equation. For the disjoining potential f_{P}, the spinodal region is infinite, i.e., in our scaling the potential predicts a break-up of all homogeneous films of a height $h_0 > \sqrt[3]{2}$. In the case of f_{S} with the parameter $\chi = 1.09$ [LGP02, TVA+09] we consider in this work, the spinodal region is bounded from above.
In contrast to f_{P}, for f_{S} one finds $h_{\mathrm{I}} \neq h_{\mathrm{II}}$ satisfying condition (3.18), i.e., two coexisting film heights. The lower film height $h_{\mathrm{I}} \approx 2.233$ is identified with the precursor film height h_{p}. Due to this fact, the thin film equation with the potential f_{S} exhibits phase separation dynamics between the two film heights h_{I} and h_{II} and therefore shows dewetting into pancake-like drops. The equation supplemented by f_{P} exhibits phase separation between dry regions and droplets with a given contact angle [Pis01]. Simulations of the dewetting dynamics in one and two dimensions are shown in figure 4.4, figure 4.5 and figure 4.6, respectively. From the dispersion relation (4.8), one can easily calculate the wavelength $\lambda_{\mathrm{P,S}}$ of the fastest growing mode at a given initial homogeneous film height h_0:

$$\lambda_{\mathrm{P,S}} = 2\pi \sqrt{-2 \left(\left. \frac{\partial^2 f_{\mathrm{P,S}}}{\partial h^2} \right|_{h_0} \right)^{-1}}. \tag{4.9}$$

In our scaling and for typical initial film heights, the wavelengths differ significantly for the two potentials, hence the simulations shown in figures 4.4 - 4.6 for the two potentials are performed on domains of a size of different orders of magnitude.

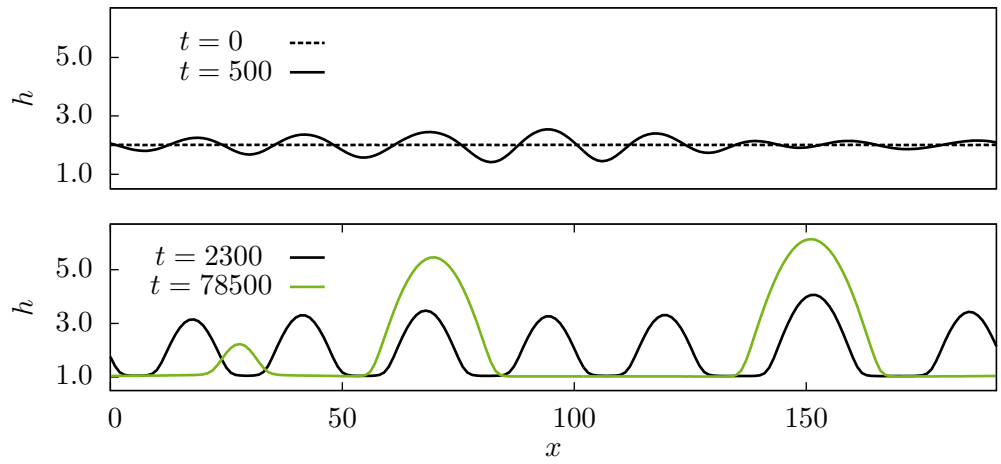

Figure 4.4.: Four snapshots of 1D numerical simulation of the dewetting dynamics exhibited by equation (4.1) with the disjoining potential f_{P}. Phase separation between regions of precursor height ($h = h_{\mathrm{p}} = 1.0$) and droplets is shown as well as the typical coarsening dynamics.

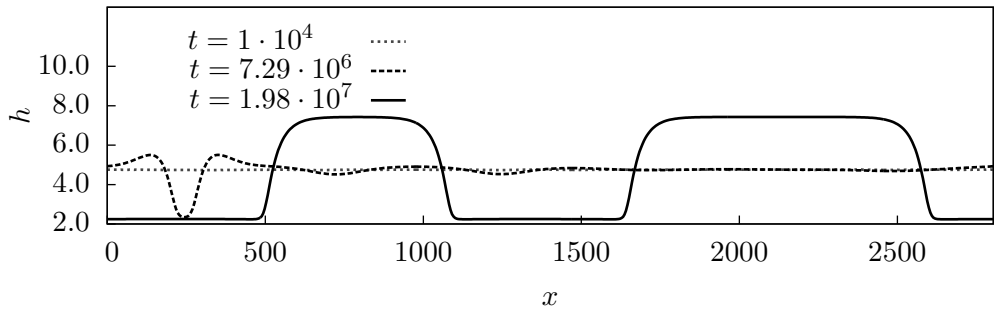

Figure 4.5.: Dewetting dynamics resulting from the disjoining potential f_S in equation (4.1). In contrast to the simulation shown in figure 4.4, phase separation into domains of different well defined film heights (given by the Maxwell construction, see figure 4.3) takes place, rather then into regions of precursor height and droplets. The result of this phase separation is the formation of pancake-like drops.

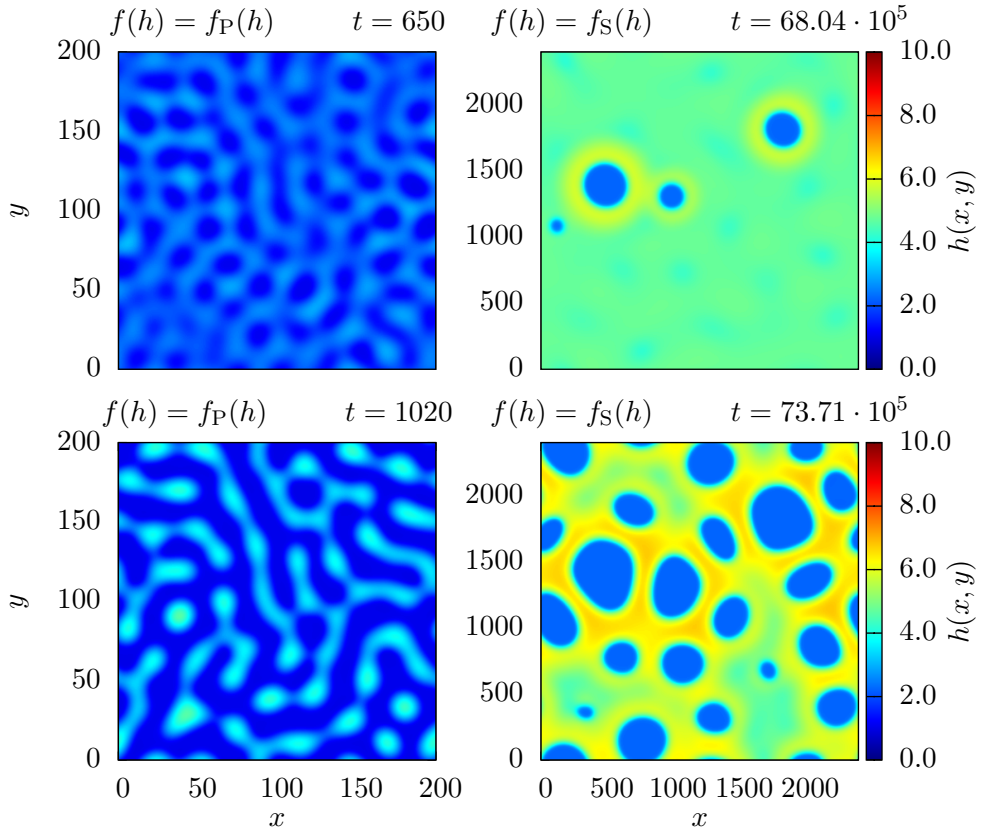

Figure 4.6.: 2D numerical simulations of equation (4.1) showing dewetting dynamics in an early stage for the different disjoining potentials f_S (right panel) and f_P (left panel).

4.2. Viscosity and Evaporation

4.2.1. Viscosity

To complete the extended equations (3.64), (3.65) for the case of non-vanishing solute concentration, we need to formulate an expression for the concentration-dependent viscosity $\eta(\phi)$ of the fluid. In the equations in question, the viscosity appears in the mobility coefficients

$$Q_{hh} = \frac{h^3}{3\eta(\phi)}; \qquad Q_{\text{diff}} = \frac{h\phi}{6\pi L^2 \eta(\phi)}. \tag{4.10}$$

For the choice of the dimensional viscosity $\eta(\phi)$, we follow [WCM03, TVA$^+$09] and define

$$\eta(\phi) = \left(1 - \frac{\phi}{\phi_r}\right)^{-2}. \tag{4.11}$$

Here, ϕ_r is the random-close-packing volume concentration of the solute, which we set to unity for the sake of simplicity. The concentration dependence above was derived in [Que77] for the case of concentrated suspensions from minimum energy dissipation considerations. Notice that it is a special case of the well known *Krieger-Dougherty* law, which states (for concentrations c):

$$\eta(c) = \eta_0 \left(1 - \frac{c}{c_{\text{r}}}\right)^{-\nu}. \tag{4.12}$$

A derivation of the Krieger-Dougherty law can be found in [Pro05]. An important feature of the choice (4.11) for the concentration dependence is that the resulting mobility coefficients (4.10) appearing in our equations tend to zero for $\phi \to 1$ due to the strongly nonlinear divergence of the viscosity.

4.2.2. Evaporation

We now wish to extend equations (3.64) and (3.65) by an additive evaporation term. The formulation of an appropriate evaporation term for thin film equations of simple liquids is not evident and the formulation of such a term for solutions is, as one might expect, even more delicate. For the case of simple fluids, in [LGP02, TVA$^+$09, Köp11], the following ansatz for the equations extended by an evaporation term is made:

$$\partial_t h = \nabla \cdot \left[Q_{hh} \nabla \frac{\delta F_{\text{SF}}}{\delta h} \right] - E_{\text{v}} \left(\frac{\delta F_{\text{SF}}}{\delta h} - \mu_{\text{v}} \right). \tag{4.13}$$

In this ansatz, μ_{v} is the chemical potential of the vapor and $E_{\text{v}} > 0$ is a constant determining the strength of the evaporation. The underlying assumption is that the evaporation is a process close to equilibrium and thus proportional to the difference of

the chemical potential of the liquid phase $\mu_\mathrm{l} := \frac{\delta F_\mathrm{SF}}{\delta h}$ and the chemical potential of the vapor phase. Equation (4.13) is an equation of Cahn-Hilliard type supplemented by an equation of *Allen-Cahn* type [AC79]. The evolution of a stable homogeneous film of height $h(t)$ is then described by the ordinary differential equation

$$\partial_t h = -E_\mathrm{v} \left(f'_\mathrm{P,S}(h) - \mu_\mathrm{v} \right). \tag{4.14}$$

The obvious fixed points h_stat are given by

$$f'_\mathrm{P,S}(h_\mathrm{stat}) - \mu_\mathrm{v} = \Pi_\mathrm{P,S}(h_\mathrm{stat}) - \mu_\mathrm{v} = 0. \tag{4.15}$$

One readily observes (see figure 4.3) that for an almost vanishing chemical potential in equation (4.13) in the case of the disjoining potential f_P, the thin film evaporates until it reaches the precursor height $h = 1.0$. This fixed point is stable.
For the case of f_S, one can consider a chemical potential μ_v below the point of the Maxwell construction (see figure 4.3, e.g. $\mu_\mathrm{v} = -0.003$ in our scaling) and obtain two stable fixed points with respect to the evaporation term. Equation (4.13) then exhibits moving front solutions between the two fixed points (figure 4.7 and [LGP02]).

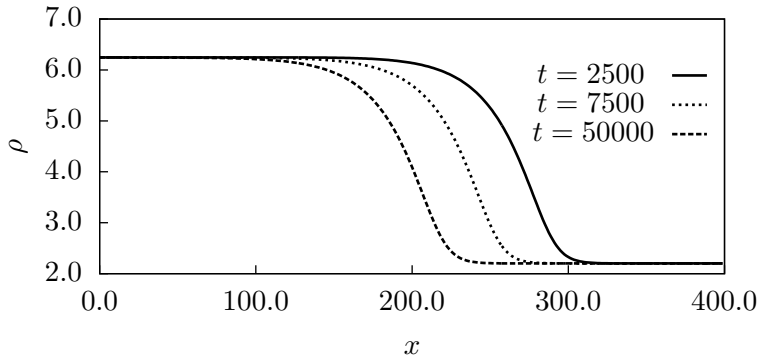

Figure 4.7.: Moving front between the two fixed points of the evaporation term, given by equation (4.15) with $\mu_v = -0.003$, $E_\mathrm{v} = 0.7$, as investigated in [LGP02].

For the case of solutions, we now wish to formulate an evaporation term which accounts for the evaporation of the solvent, whereas the solute is non-volatile. In [FAT11, FAT12], where evaporating solutions are described, the authors assume the same evaporation term (4.13) as for a simple liquid. This ansatz is of course only a minimal model, since the evaporation term in (4.13) does not account in any way for the amount of solute present in the liquid. Therefore, this ansatz, although it yields a relatively simple evaporation term, fails for large concentrations in our case, where it might lead to concentrations larger than unity.
In analogy to the local height of the solvent $\Psi(\mathbf{x}, t)$, it is useful to introduce $\rho(\mathbf{x}, t)$ as the local height of the solute such that

$$\rho(\mathbf{x}, t) = h(\mathbf{x}, t) - \Psi(\mathbf{x}, t). \tag{4.16}$$

If we aim for an evaporation term which does not permit concentrations larger than unity, this is equivalent to the request of an evaporation term which leads to fixed points in ρ which are larger than zero. In this work, we use the following ansatz for the extension of equations (3.64), (3.65) in their gradient formulation, which is also shortly discussed in [Thi11]:

$$\begin{aligned}\partial_t h &= \nabla \cdot \left[Q_{hh} \nabla \frac{\delta F}{\delta h} + Q_{h\Psi} \nabla \frac{\delta F}{\delta \Psi} \right] - E_\mathrm{v} \left(\frac{\delta F}{\delta h} - \mu_\mathrm{v} \right), \\ \partial_t \Psi &= \nabla \cdot \left[Q_{\Psi h} \nabla \frac{\delta F}{\delta h} + Q_{\Psi\Psi} \nabla \frac{\delta F}{\delta \Psi} \right].\end{aligned} \tag{4.17}$$

This ansatz is a straight-forward generalization of (4.13), where we now consider the difference between the chemical potential μ_v of the vapor and the chemical potential μ_s of the solvent, which reads

$$\mu_\mathrm{s} := \frac{\delta F[h,\Psi]}{\delta h} = \frac{\delta \mathcal{F}[h,\phi]}{\delta h} - \frac{\phi}{h} \frac{\delta \mathcal{F}[\phi,h]}{\delta \phi}. \tag{4.18}$$

An easy calculation in analogy to (3.46) shows that

$$\tilde{F} = F - \int_A \mu_\mathrm{v} h \, dx^2 \tag{4.19}$$

is a Lyapunov functional of equation (4.17). For our extended free energy functional (3.58), the chemical potential of the solvent is given by the variations (3.62) and (3.63). For the case of a homogeneous thin film, it therefore reduces to

$$\mu_\mathrm{s} = f'(h) + g(\phi) - \phi g'(\phi). \tag{4.20}$$

The term $g(\phi) - \phi g'(\phi)$ corresponds to the *osmotic pressure* of the solute as it is introduced, e.g., for the already mentioned Flory-Huggins free energy in [deG79]. We will discuss explicitly the evaporation term for the disjoining potential f_P, which will be used in the following chapter. In this case, the evolution of the solute height for homogeneous films reads

$$\partial_t \rho = -E_\mathrm{v} \left(\Pi_\mathrm{P}(\Psi + \rho) + L^3 E_\mathrm{T} \left(\alpha \left(\frac{\Psi}{\rho + \Psi} \right)^2 + \ln \left(\frac{\rho}{\Psi + \rho} \right) \right) - \mu_\mathrm{v} \right). \tag{4.21}$$

Here, the solute height Ψ has to be considered as a constant. It is easily seen that the logarithmic osmotic pressure contribution diverges to $-\infty$ for $\rho \to 0$. It therefore ensures fixed points $\rho_\mathrm{stat} > 0$ for all solute heights Ψ. However, the parameters μ_v and $E_\mathrm{T} L^3$ need to be well adjusted to ensure physically meaningful values of these fixed points. Plots of the right-hand side and a numerical solution of equation (4.21) are shown in figure (4.8) and (4.9), respectively, for parameters which will be used in the

following chapter ($E_T L^3 = 0.1538$ and $\mu_\mathrm{v} = -0.3077$)[1]. For non-homogeneous films, the full evaporation term reads:

$$\delta_\mathrm{ev} = -E_\mathrm{v}\left(f'(h) - \Delta h + g(\phi) - \phi g'(\phi) + \frac{\gamma}{2}(\boldsymbol{\nabla}\phi)^2 + \gamma\frac{\phi}{h}\boldsymbol{\nabla}\cdot(h\boldsymbol{\nabla}\phi) - \mu_\mathrm{v}\right). \quad (4.22)$$

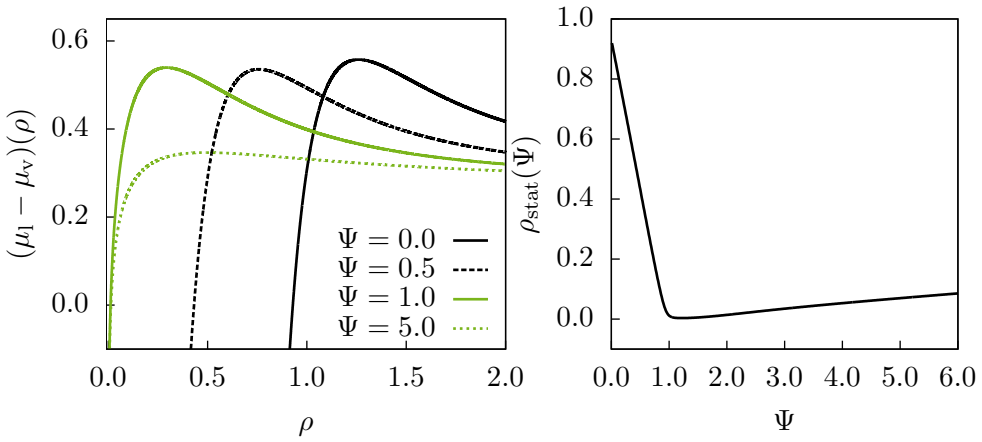

Figure 4.8.: Left: Plot of the evaporation term as a function of ρ for $\alpha = 2.3$, omitting the factor $-E_\mathrm{v}$. Right: Fixed points in ρ as a function of the constant solute height Ψ.

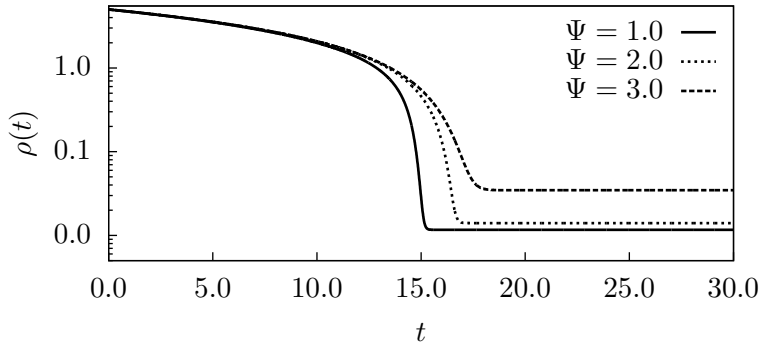

Figure 4.9.: Numerical simulation of equation (4.21) for different solute heights Ψ, $\alpha = 2.3$ and $E_\mathrm{v} = 1.0$.

[1] We are aware of the fact that the order of magnitude of μ_v is high compared to the maximum of the disjoining potential f_P. Nevertheless, these parameters have to be chosen mainly for numerical reasons, since for lower values of μ_v, fixed points in ρ very close to zero occur, which we are not able to treat numerically for 2D simulations due to the divergent logarithm in the evaporation term.

4.3. Linear Stability

In this section, we will investigate the linear stability of homogeneous solutions of the full equations (3.64) and (3.65), including the evaporation term discussed in the previous section. To perform this linear stability analysis, the use of the gradient formulation (4.17) is very helpful. For a similar gradient system, excluding evaporation terms, a quite general stability analysis is shown in [PBMT05]. We linearize equation (4.17) about homogeneous states h_0, Ψ_0, which correspond to fixed points of the evaporation term, i.e.,

$$\left.\frac{\delta F}{\delta h}\right|_{h_0,\Psi_0} - \mu_\mathrm{v} = 0. \tag{4.23}$$

Since we are only concerned with linear terms, it is sufficient to consider the following equation as a starting point:

$$\begin{pmatrix} \partial_t h \\ \partial_t \Psi \end{pmatrix} = \left(\underline{\mathbf{Q}}\Delta + \underline{\mathbf{E}}\right) \begin{pmatrix} \frac{\delta F}{\delta h} \\ \frac{\delta F}{\delta \Psi} \end{pmatrix}, \tag{4.24}$$

where we introduced the negative semidefinite evaporation matrix

$$\underline{\mathbf{E}} := \begin{pmatrix} -E_\mathrm{v} & 0 \\ 0 & 0 \end{pmatrix}. \tag{4.25}$$

To perform the calculations in a more general framework, we furthermore define

$$\tilde{f}(h,\Psi) = f_{\mathrm{S,P}}(h) + hg(h,\Psi). \tag{4.26}$$

We now perform the ansatz $h(\mathbf{x},t) = h_0 + \eta(\mathbf{x},t)$, $\Psi(\mathbf{x},t) = \Psi_0 + \xi(\mathbf{x},t)$, where $\eta,\ \xi$ are small perturbations.
The first order in $\xi,\ \eta$ of the variations of F with respect to $h,\ \Psi$ then read

$$\frac{\delta F}{\delta h} = \text{const.} + \left.\frac{\partial^2 \tilde{f}}{\partial h^2}\right|_{h_0,\Psi_0} \eta + \left.\frac{\partial^2 \tilde{f}}{\partial h \partial \Psi}\right|_{h_0,\Psi_0} \xi - \Delta\eta - \gamma\frac{\Psi_0^2}{h_0^3}\Delta\eta + \gamma\frac{\Psi_0}{h_0^2}\Delta\xi + \text{h.o.t.}, \tag{4.27}$$

$$\frac{\delta F}{\delta \Psi} = \text{const.} + \left.\frac{\partial^2 \tilde{f}}{\partial \Psi^2}\right|_{h_0,\Psi_0} \xi + \left.\frac{\partial^2 \tilde{f}}{\partial \Psi \partial h}\right|_{h_0,\Psi_0} \eta - \frac{\gamma}{h_0}\Delta\xi + \gamma\frac{\Psi_0}{h_0^2}\Delta\eta + \text{h.o.t.}\ . \tag{4.28}$$

We insert these variations combined with a Fourier ansatz

$$\begin{pmatrix} \eta(\mathbf{x},t) \\ \xi(\mathbf{x},t) \end{pmatrix} = \begin{pmatrix} \eta_k(t) \\ \xi_k(t) \end{pmatrix} e^{\mathrm{i}\mathbf{k}\cdot\mathbf{x}} \tag{4.29}$$

into equation (4.24) and obtain the system of ODEs

$$\begin{pmatrix} \partial_t \eta_k(t) \\ \partial_t \xi_k(t) \end{pmatrix} = \left(-k^2 \underline{\mathbf{Q}} + \underline{\mathbf{E}}\right) \underline{\mathbf{J}} \begin{pmatrix} \eta_k(t) \\ \xi_k(t) \end{pmatrix}. \tag{4.30}$$

The Jacobian matrix $\underline{\mathbf{J}}$ reads:

$$\underline{\mathbf{J}} = \begin{pmatrix} \frac{\partial^2 \tilde{f}}{\partial h^2} + k^2 + \gamma \frac{\Psi_0^2}{h_0^3} k^2 & \frac{\partial^2 \tilde{f}}{\partial h \partial \Psi} - \gamma \frac{\Psi_0}{h_0^2} k^2 \\ \frac{\partial^2 \tilde{f}}{\partial \Psi \partial h} - \gamma \frac{\Psi_0}{h_0^2} k^2 & \frac{\partial^2 \tilde{f}}{\partial \Psi^2} + \frac{\gamma}{h_0} k^2 \end{pmatrix}. \tag{4.31}$$

In the following, we consider the case $k \neq 0$. The fixed point $(0,0)^{\mathrm{T}}$ of the ODEs (4.30) is stable if and only if $\underline{\tilde{\mathbf{Q}}}\underline{\mathbf{J}}$ is negative semidefinite, where $\underline{\tilde{\mathbf{Q}}} := -k^2\underline{\mathbf{Q}} + \underline{\mathbf{E}}$. Inserting the definition (4.26) and some calculations which are readily performed yield the following matrix $\underline{\mathbf{J}}$:

$$\underline{\mathbf{J}} = \begin{pmatrix} (f''_{\mathrm{P,S}}(h_0) + k^2) + \frac{\phi_0^2}{h_0}\left(g''(\phi_0) + \gamma\ k^2\right) & -\frac{\phi_0}{h_0}\left(g''(\phi_0) + \gamma\ k^2\right) \\ -\frac{\phi_0}{h_0}\left(g''(\phi_0) + \gamma\ k^2\right) & \frac{1}{h_0}(g''(\phi_0) + \gamma\ k^2) \end{pmatrix}. \tag{4.32}$$

In this matrix, the terms

$$S_h := -(f''_{\mathrm{P,S}}(h_0) + k^2); \qquad S_\phi := -(g''(\phi_0) + \gamma\ k^2) \tag{4.33}$$

determine the sign of the eigenvalues of $\underline{\mathbf{J}}$. Obviously, these two terms have a simple interpretation of their own: $k^2 S_h$ and $k^2 S_\Phi$ are proportional to the dispersion relations of the simple thin film equation (4.1) and a Cahn-Hilliard equation in ϕ with the free energy density $g(\phi)$, respectively.
The signs of the eigenvalues of $\underline{\tilde{\mathbf{Q}}}\underline{\mathbf{J}}$ can be deduced from the trace and the determinant of the matrix. Since for $k \neq 0$ the matrix $\underline{\tilde{\mathbf{Q}}}$ is negative definite, the sign of the determinant and and the thresholds of instability are fixed solely by the matrix $\underline{\mathbf{J}}$. For the trace of $\underline{\tilde{\mathbf{Q}}}\underline{\mathbf{J}}$ and the determinant of $\underline{\mathbf{J}}$, simple calculations yield:

$$\mathrm{Tr}[\underline{\tilde{\mathbf{Q}}}\underline{\mathbf{J}}] = E_{\mathrm{v}}\left(S_h + \frac{\phi_0^2}{h_0} S_\phi\right) + k^2\left(\frac{h_0^3}{3\eta_0} S_h + \frac{Q_{\mathrm{diff}}}{h_0} S_\phi\right); \quad \mathrm{Det}[\underline{\mathbf{J}}] = \frac{1}{h_0} S_h S_\Phi. \tag{4.34}$$

At least one of the eigenvalues of $\underline{\tilde{\mathbf{Q}}}\underline{\mathbf{J}}$ is positive and $(0,0)^{\mathrm{T}}$ is an unstable fixed point of the linearized equations (4.30), if $\mathrm{Det}[\underline{\mathbf{J}}] < 0$ or $\mathrm{Tr}[\underline{\tilde{\mathbf{Q}}}\underline{\mathbf{J}}] > 0$. We therefore end up with the quite trivial result that our coupled equations (4.17) are unstable if

(a) The homogeneous height in the thin film equation (4.1) is unstable and the concentration in the Cahn-Hilliard equation for the concentration is stable or vice versa: $(S_h > 0,\ S_\phi < 0) \vee (S_h < 0,\ S_\phi > 0) \Rightarrow\ \mathrm{Det}[\underline{\mathbf{J}}] < 0$.

(b) Both height and concentration are unstable in their respective decoupled equation: $S_h > 0,\ S_\phi > 0 \Rightarrow\ \mathrm{Tr}[\underline{\tilde{\mathbf{Q}}}\underline{\mathbf{J}}] > 0$.

In the non-evaporative case, the growth rate $\nu_\phi(k)$ and the fastest growing wavelength $\lambda_{\max,\phi}$ of the linear instability in ϕ read

$$\nu_\phi(k) = \frac{\phi_0}{6\pi L^2 \eta(\phi_0)}(-g''(\phi)k^2 - \gamma k^4); \qquad \lambda_{\max,\phi} = \sqrt{\frac{-8\pi^2\gamma}{g''(\phi_0)}}. \tag{4.35}$$

If both height and concentration are stable in their respective decoupled Cahn-Hilliard equations, the coupled equations are stable too. For the positive definite mobility matrix, the stability is determined by the structure of the free energy functional $\mathcal{F}[h, \phi]$, where the coupling between ϕ and h is weak in our case. A stronger coupling, which also induces new cooperative instabilities can be observed for disjoining potentials, which are concentration-dependent [TTL13]. Since one main goal of this work is to write a simple model for the structure formation at the contact line, we do not consider this coupling here. In [Cla04], a linear stability condition is derived only by considering a general free energy functional of the type $\mathcal{F} = \int_A f(\phi, h) + h f_\mathrm{b}(\phi)$. This stability criterion can be reproduced for our gradient system. This shows the thermodynamical consistency of this formulation, which goes beyond the fact that h and Ψ are conserved.

4.4. Dynamics of Thin Solution Layers

4.4.1. Dewetting and Phase Separation

In analogy to the calculations shown for the van der Waals gas, we now investigate the non-gradient part of the free energy functional (3.58) with respect to the possibility of phase coexistence in both h (dewetting) and Ψ. In the system of equations for h and ϕ (3.65), it is clear that the phases in h will be solely defined by the disjoining potential, since the non-gradient coupling of ϕ into the evolution equation for h occurs only through the mobility. We will nevertheless shortly present the general calculations which for more complicated free energy functionals will reveal cooperative phases in ϕ and h. We consider the energy of a system, where the fields have the values $h_1,\ h_2$ and $\phi_1,\ \phi_2$ on the areas $A_1,\ A_2$. This energy has to be minimized with respect to $h_i,\ \phi_i$ and A_i under the constraints of overall volume-, solute volume- and area conservation. The constraints are implemented in terms of lagrangian multipliers [HW91] and the expression to be minimized reads

$$\begin{aligned} e_\mathrm{ps} :=& A_1\tilde{f}(\phi_1, h_1) + A_2\tilde{f}(\phi_2, h_2) + \lambda_1\ (\phi_1 h_1 A_1 + \phi_1 h_1 A_1) \\ &+ \lambda_2\ (h_1 A_1 + h_2 A_2) + \lambda_3(A_1 + A_2). \end{aligned} \tag{4.36}$$

The minimalization of this energy term with respect to all arguments leads to the following equalities:

$$\tilde{f}(\phi_1, h_1) - h_1 \partial_h \tilde{f}(\phi_1, h_1) = \tilde{f}(\phi_2, h_2) - h_1 \partial_h \tilde{f}(\phi_2, h_2), \tag{4.37}$$

$$\partial_h \tilde{f}(\phi_1, h_1) - \frac{\phi_1}{h_1} \partial_\phi \tilde{f}(\phi_1, h_1) = \partial_h \tilde{f}(\phi_2, h_2) - \frac{\phi_2}{h_2} \tilde{f}(\phi_2, h_2), \tag{4.38}$$

$$\frac{1}{h_1} \partial_\phi \tilde{f}(\phi_1, h_1) = \frac{1}{h_2} \partial_\phi \tilde{f}(\phi_2, h_2). \tag{4.39}$$

This system of equations is also investigated in [Tod13] for the same purpose as here. To close the system of equations, we follow [Tod13] and explicitly formulate the conservation of solute and volume and obtain as a fourth equation

$$\frac{h_0 \phi_0 - \phi_2 h_2}{h_1 \phi_1 - \phi_2 h_2} = \frac{h_0 - h_2}{h_1 - h_2}. \tag{4.40}$$

In our case, the equations (4.37)-(4.39) yield

$$f(h_1) - h_1 f'(h_1) = f(h_2) - h_2 f'(h_2), \tag{4.41}$$

$$f'(h_1) + g(\phi_1) - \phi_1 g'(\phi_1) = f'(h_2) + g(\phi_2) - \phi_2 g'(\phi_2), \tag{4.42}$$

$$g'(\phi_1) = g'(\phi_2). \tag{4.43}$$

In these equations, one can identify the equations (3.18) for h and ϕ for the case of decoupled free energies in h and ϕ, which are now coupled through equation (4.42). In addition and most importantly, the phases ϕ_i, h_i are coupled through the conservation constraint in Ψ, which leads to equation (4.40). Due to this equation, phases in ϕ and h, which may coexist in the decoupled phase (e.g. the two coexisting film heights in h for the case of the Sharma potential) are in general not coexisting for the coupled system (in the way assumed here, i.e., where h_i, ϕ_i occupy the same domains A_i). For the special case of $h_1 = h_2$, which will occur if h_0 is chosen outside of the binodal region of h, solutions ϕ_i to the equations

$$g'(\phi_1) = g'(\phi_2); \qquad g(\phi_1) - \phi_1 g'(\phi_1) = g(\phi_2) - \phi_2 g'(\phi_2) \tag{4.44}$$

are obviously also solutions to the equations (4.41)-(4.43). The conservation constraints corresponding to equation (4.40), which is of course not defined for $h_1 = h_2$, can be met for an appropriate choice of A_1, A_2. Solutions to equation (4.44), i.e., the classical binodal lines for the regular solution free energy (3.60), are shown in figure 4.10.

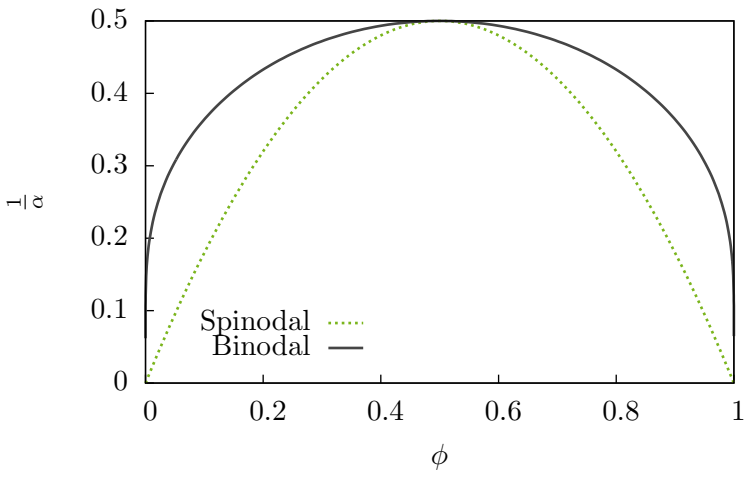

Figure 4.10.: Binodal and spinodal lines for the regular solution free energy (3.60).

1D numerical simulations of the full equations (3.64), (3.65) without evaporation in a regime where phase separation, as well as dewetting, occurs are shown in figures 4.11 and 4.12, respectively. The Sharma potential (4.4) is used as the disjoining potential. Although it was derived in another context, in these equations the parameter γ can be used to adjust the coupling strength of the gradient terms in ϕ to the advective flux. It then corresponds to a scaled coupling parameter of the Cauchy stress tensor in the Navier-Stokes equation which was mentioned in section 3.6. Here we choose a very weak coupling ($\gamma = 1 \cdot 10^{-4}$), the nonlinear effects of a strong coupling will be discussed in the next section. For a fixed parameter γ, the growth rate of the instability in ϕ and the corresponding typical wavelength can then be adjusted through the parameters $\frac{1}{\mathrm{Pe}}$ and $E_{\mathrm{T}}L^3$. In figures 4.11 and 4.12, one observes that, as stated above, no cooperative phases in h and ϕ are formed. As expected, the phase decomposition in the two fields rather occurs into the same phases as in the decoupled case.
Nevertheless, the coarsening dynamics are now coupled through the mass conservation constraint. The detailed investigation of these dynamics is an interesting topic which should be addressed quantitatively using a simplified bulk free energy (i.e. the classical polynomial Cahn-Hilliard free energy) as in ([NT10]) instead of the full bulk free energy (3.60). However, this does not lie in the scope of the present work.

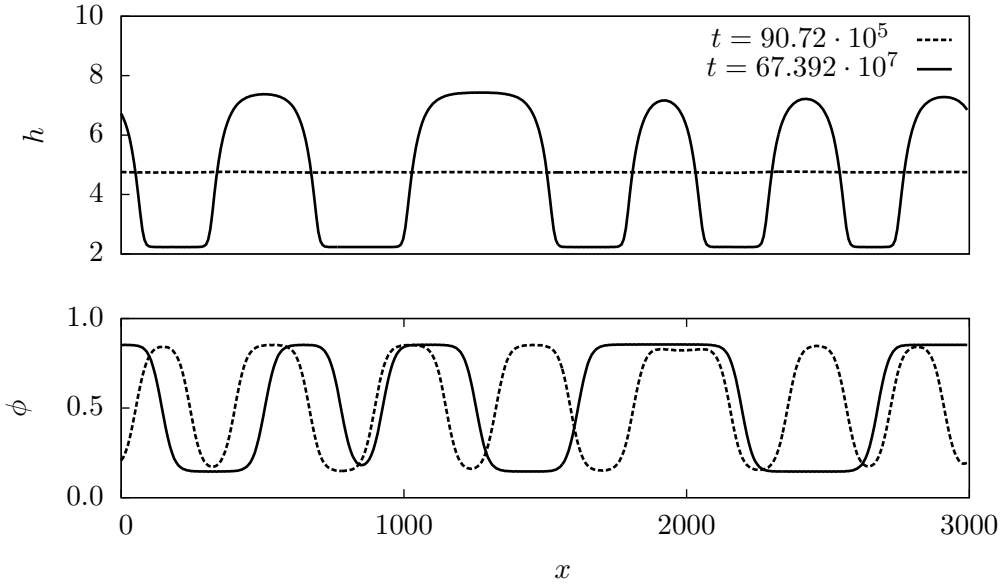

Figure 4.11.: Dewetting and phase separation of a thin solution layer as a result of equations (3.64) for $\alpha = 2.5$, $E_\mathrm{T} L^3 = 0.1 \cdot 10^{-7}$, $\mathrm{Pe}^{-1} = 0.2\overline{7}$. For these parameters, the phase separation is well advanced when the dewetting starts.

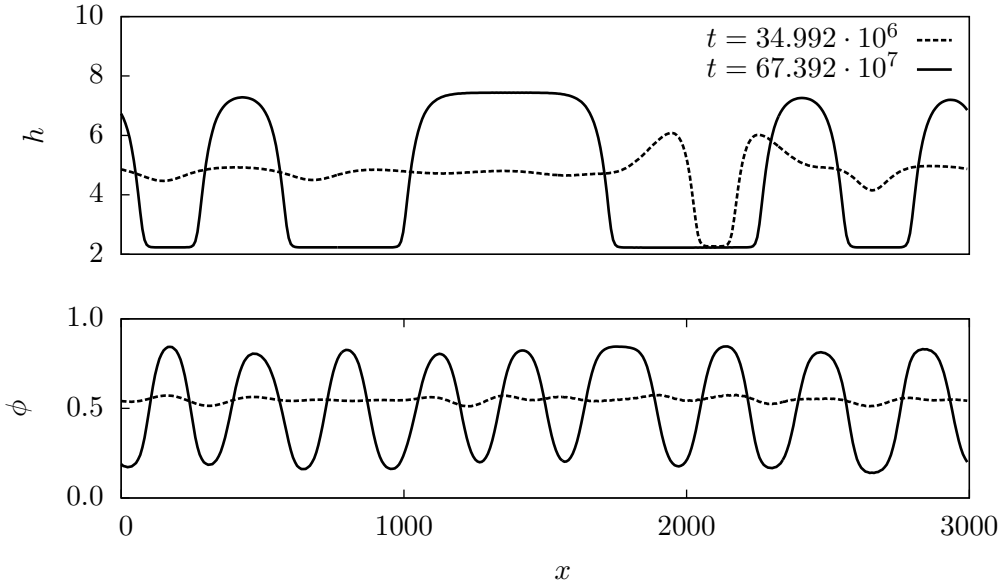

Figure 4.12.: Dewetting and phase separation for $\alpha = 2.5$, $E_\mathrm{T} L^3 = 0.1 \cdot 10^{-7}$, $\mathrm{Pe}^{-1} = 1.3\overline{8} \cdot 10^{-3}$. Here, the dewetting instability occurs on a smaller time-scale compared to the instability of the phase decomposition.

4.4.2. Nonlinear Coupling

A linear stability analysis as performed in section 4.3 shows no coupling between the fields h and ϕ. Nevertheless, due to the gradient contributions of ϕ in the advective flux

$$\mathbf{J}_{\text{adv}} = -Q_{hh}\left(\nabla\left(-\Delta h + f'(h) + \frac{\gamma}{2}(\nabla\phi)^2\right) + \frac{\gamma}{h}\nabla\cdot(h\nabla\phi)\nabla\phi\right), \tag{4.45}$$

for large values of γ, instabilities in ϕ can have a significant effect on the height profile $h(\mathbf{x})$. As shown in figure 4.13, gradients in ϕ induce cusp-like notches in the height profile, for initial heights, which are metastable or even stable in the decoupled case. This phenomenon is discussed in detail in [NT10], where the authors consider a disjoining pressure of van der Waals type which is regularizing for all film heights.
In figures 4.13 and 4.14, 1D numerical simulations are shown where phase separation occurs in a film of height $h_0 = 2.5$ and $h_0 = 2.55$, respectively. For the Sharma potential, these film heights lie both in the metastable regime. The larger film height is very close to the limit of instability and, as one can observe in figure 4.14, the notches produced by the gradients in ϕ eventually lead to the nucleation and growth of elevated drops. The growth of the drops is coupled to the coarsening of the structures in the concentration field. The drops do not necessarily grow in regions of low concentration, but the concentration dependence of the mobility Q_{hh} enhances this behavior. Nevertheless, the boundaries of the drops are always located at the interphases of the structures in ϕ.

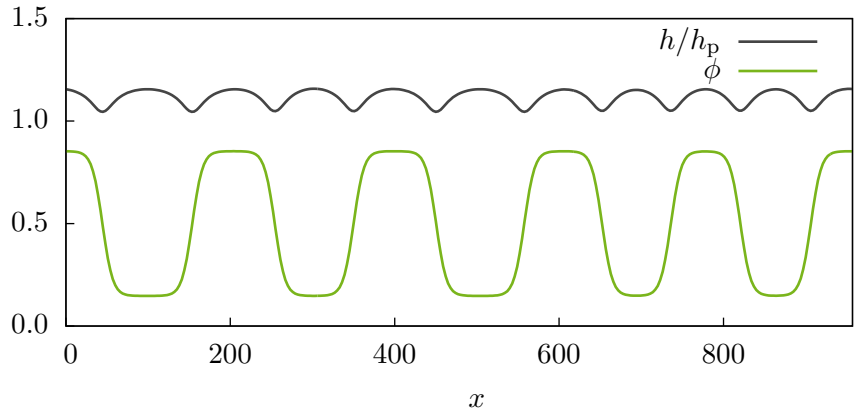

Figure 4.13.: 1D numerical simulation of equations (3.64) and (3.65) showing the nonlinear coupling of gradients in the concentration field to the height profile. At the interfaces in ϕ (green curve), cusp-like structures in h (black curve) are formed. The parameters are $\alpha = 2.3$, $TL^3 = 0.1$, $h_0 = 2.5$, $c_0 = 0.5$, $\text{Pe}^{-1} = 0.1$, $\gamma = 10$.

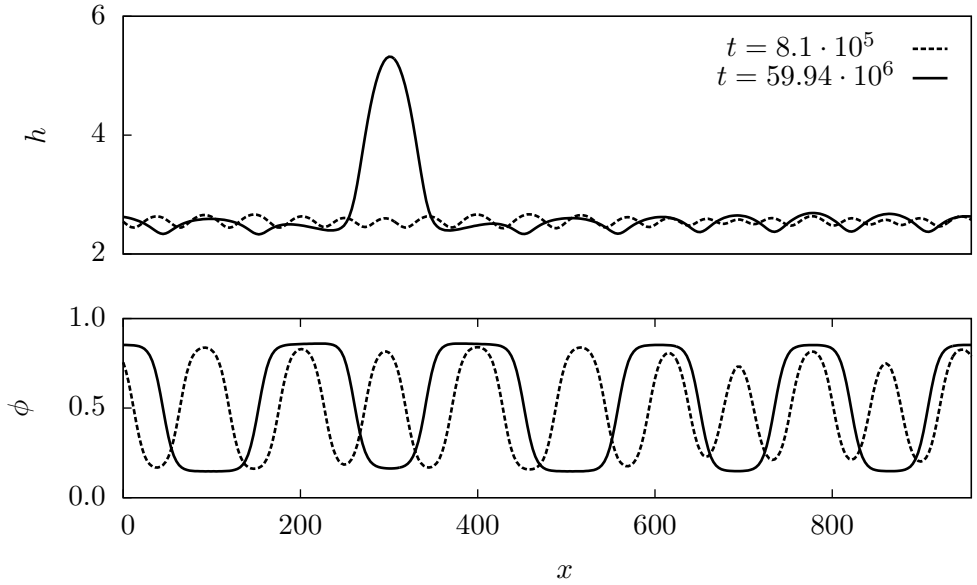

Figure 4.14.: 1D numerical simulation of equations (3.64) and (3.65), showing the growth of a drop, starting with a film of height $h_0 = 2.55$. This film height is at the edge of the metastable regime and the growth is induced by the coupling to the phase separation in ϕ. All parameters except for the initial film height are as denoted in figure 4.13.

5. Transfer onto Substrates

As mentioned in the introductory chapter, this work represents a first step towards the aim of a theoretical description of complicated dendritic-like structures formed in dip-coating experiments. It is evident that the thin film equations derived in chapter 3 can not be used to exactly or even quantitatively describe solutions like the one employed in the dip-coating experiments performed in Münster [LGS$^+$10]. Nevertheless, in this chapter some first results on structures formed at the meniscus by evaporation-induced phase separation will be presented. In particular, we show that depending on the initial concentration and the pulling speed different periodic structures are formed. In addition, the resemblance to structures formed by directional quenching in the classical Cahn-Hilliard equation is discussed.
In all the simulations shown in this chapter, we chose the laboratory frame as the frame of reference. For a substrate which is pulled out of a liquid bath with a constant velocity v, this implies the inclusion of an advective term in our equations (3.64) and (3.65). This advective term was included through the boundary conditions in the derivation of the basic equations (2.61) and (2.62) in chapter 2. The full equations considered in this chapter combine the conservative, extended equations (3.64) and (3.65) with the evaporation term δ_{ev} given by (4.22) and the advection term mentioned above. Writing the conservative part in the gradient formulation, the full equations read:

$$\begin{aligned}\partial_t h &= \nabla\cdot\left[Q_{hh}\nabla\frac{\delta F}{\delta h}+Q_{h\Psi}\nabla\frac{\delta F}{\delta\Psi}\right]-E_{\mathrm{v}}\left(\frac{\delta F}{\delta h}-\mu_{\mathrm{v}}\right)-\mathbf{v}\cdot\boldsymbol{\nabla}h,\\ \partial_t(h\phi) &= \nabla\cdot\left[Q_{\Psi h}\nabla\frac{\delta F}{\delta h}+Q_{\Psi\Psi}\nabla\frac{\delta F}{\delta\Psi}\right]-\mathbf{v}\cdot\boldsymbol{\nabla}(h\phi).\end{aligned}\tag{5.1}$$

The disjoining potential f_{P} given by equation (4.3) was employed in this chapter. Throughout the chapter, the parameters Pe=0.5, $E_T L^3 = 0.01$, $E_v = 0.01$, $\mu_v = -0.02$ and, if not denoted otherwise, $\gamma = 0.01$ were chosen.[1]

[1] In this chapter , we rescale our basic equations for numerical reasons, such that $f(h) = A(1/h^3 - 1/h^6)$, where $A = 0.065$. All the parameters, as well as length and time scales, appearing in this chapter must therefore be rescaled according to $x' = \sqrt{A}x$, $t' = A^2 t$, $v' = A^{-3/2}v$, $(E_T L^3)' = \frac{1}{A}E_T L^3$, $\mathrm{Pe}^{-1} = A\mathrm{Pe}'^{-1}$, $\mu_v' = \frac{1}{A}\mu_v$, $E_v' = \frac{1}{A}E_v$ in order to obtain the parameters corresponding to the scaling outline in the previous chapter (denoted by a prime).

5.1. Boundary- and Initial Conditions

In order to describe the deposition process in dip-coating experiments, one first needs to formulate appropriate boundary conditions. Since the meniscus arises from a bath of solution, the natural boundary condition mimicking the transfer process would include

$$\lim_{y\to 0} \partial_y h(x,y) = \infty, \tag{5.2}$$

when the bath is situated at $y = 0$ (see also figure 5.1). Such a boundary condition is very hard to treat numerically. In addition, a description of the full meniscus starting from the bath would necessitate the inclusion of very large film heights near $y = 0$. Mainly due to the nonlinearities in h in the disjoining pressure term, this would also cause major problems in the numerical framework. For these reasons, we content ourselves with the modeling of the meniscus through the following boundary conditions:

$$h(x,y)|_{y=0} = h_0; \qquad \partial_y^2 h(x,y)|_{y=0} = 0; \qquad \partial_y^3 h(x,y)|_{y=0} = 0. \tag{5.3}$$

$$\partial_y h(x,y)|_{y=L} = 0; \qquad \partial_y^2 h(x,y)|_{y=L} = 0; \qquad \partial_y^3 h(x,y)|_{y=L} = 0; \tag{5.4}$$

Here, the main assumption is that the boundary value of the height can be fixed to h_0 at a given position which does not correspond to the surface of the bath (see figure 5.1). For our numerical treatment, three boundary conditions are required in the non-periodic case, since the treatment is based on finite-difference approximations of the spatial derivatives. For details, the reader is referred to the appendix. We therefore demand the second and third derivative in y-direction to vanish at the lower boundary and the corresponding first, second and third derivatives to vanish at the upper boundary. These conditions imply a certain degree of smoothness at the boundaries. Finally it seems natural to impose the boundary conditions (5.3) and (5.4) also for the field $\phi(\mathbf{x})$. Notice that very similar boundary conditions are also used in [Köp11] for the modeling of the Langmuir-Blodgett transfer. In our case, these boundary conditions are of course not completely accurate and a future task would be to derive more rigorous boundary conditions in order to capture more precisely the hydrodynamics of the meniscus.
The initial conditions are chosen as

$$\phi(\mathbf{x},0) = \phi_0; \qquad h(\mathbf{x},0) = \frac{1}{2}(h_p - h_0)\,\tanh\left(\frac{(y-a)}{b}\right), \tag{5.5}$$

i.e., the initial concentration is chosen to be constant throughout the domain of simulation whereas the initial film height $h(x,0)$ is chosen as an analytic function which is similar to the meniscus obtained in the simulations. As it should be the case for the meniscus, the function connects the initial height h_0 and the precursor height h_p. The steepness and width of the transition can be adjusted by the parameters a and b. The particular choice of the parameters is quite unimportant, as long as the film height relaxes to the natural meniscus-shape during the simulations.

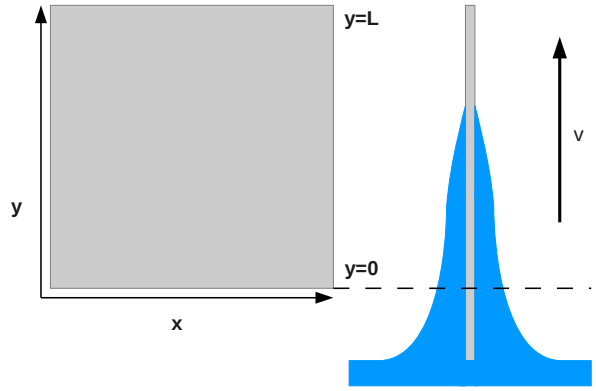

Figure 5.1.: Sketch of the meniscus in a dip-coating experiment and of the respective simulation domain considered in this chapter. The coordinates (x, y) denote the position in the plane spanned by the substrate of the length L. By using the boundary conditions (5.3), we assume that the film height h is fixed to a constant value h_0 at the position $y = 0$ in the frame of reference of the laboratory (dashed line).

5.2. Transfer from an Ideal Solution

As a first example, we consider the transfer process for vanishing values of E_J, i.e. for the case $\alpha = 0$, $\gamma = 0$ in the extended free energy functional (3.58). In this case, no solute-solvent demixing (i.e., phase separation in the concentration field) occurs and a layer of homogeneous concentration is transferred onto the substrate. Furthermore, after a sufficiently long simulation time, a static meniscus is formed, whose shape is determined by the evaporation rate, the pulling speed, the capillary forces (which are fixed in our scaling) and the initial film height. In figure 5.2, the meniscus as well as the corresponding concentration profile are shown for two different initial concentrations. Note that for the higher initial concentration, the evaporation is stopped due to the osmotic contributions in equation (4.22), which are discussed in chapter 4. For an evaporation term without these contributions, the concentration would exceed unity at the meniscus. The height of the transferred precursor is approximately constant for values $\Psi \in [0, 1]$, as one can see in figure 4.8. For $\Psi > 1$, the precursor height increases with the amount of solute.

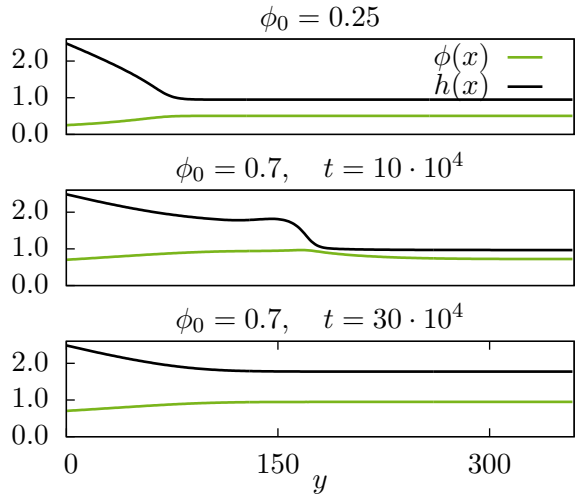

Figure 5.2.: Snapshots of simulations of equations (5.1) for $\gamma = 0$, $\alpha = 0$. Top: Height profile forming a static meniscus (black) and static concentration profile (green) for $\phi_0 = 0.25$. Middle: For the case $\phi_0 = 0.7$, part of the initial meniscus is carried away, since the evaporation term and the mobility vanish for $\phi \to 1$.
Bottom: static meniscus and concentration profile obtained for $\phi_0 = 0.7$ and longer simulation times. All curves are taken from 2D simulations at $x = L_x/2$, where $L_x = 20$ is the domain size in x-direction.

5.3. Formation of Periodic Patterns

5.3.1. Stripe Patterns

We will now consider the case $E_J \neq 0$. The parameter α associated with the interaction energy is chosen as $\alpha = 2.3$, such that phase-coexistence in the concentration field is possible (see figure 4.10). If the initial concentration is high enough and the concentration reaches the spinodal range due to the evaporation in the meniscus, a spinodal instability occurs during the transfer process. Physically speaking, the solute and the solvent demix when a critical concentration is reached. This phase separation is now directed by the transfer process and a first region of high concentration is formed parallel to the contact line. As a consequence of mass conservation, behind this first region of high concentration a region of low concentration is formed. Note however that by mass conservation, we mean the conservation of $\Psi(x)$ rather than of $\phi(x)$. The form of the meniscus is therefore relevant for the process of phase separation. As the kink-antikink structure is advected, the process repeats itself periodically resulting in a pattern of stripes which are aligned parallel to the meniscus. It has to be emphasized that the wavenumber of the structures formed at the meniscus does not correspond to the wavenumber of the fastest growing mode in the corresponding spinodal decomposition but is determined by the dynamical process described above. The dependence of the wavenumber k of the structures on the transfer velocity v is shown in figure 5.3.

The absolute height $h = \rho + \Psi$ of the transferred film is approximately equal for both phases, as the amount of solute Ψ is always smaller than unity. The meniscus of the height field remains almost static during the process of pattern formation.
In figure 5.4, 2D numerical simulations are shown exhibiting the formation of stripe patterns and their dependence on the initial concentration ϕ_0. As one can readily see, the width of the stripes of high concentration is increased monotonically with the initial concentration.
Finally, it is important to emphasize that the periodic stripe patterns do no correspond to a minimum of the Lyapunov functional given by equation (4.19) and are subjected to slow coarsening dynamics.

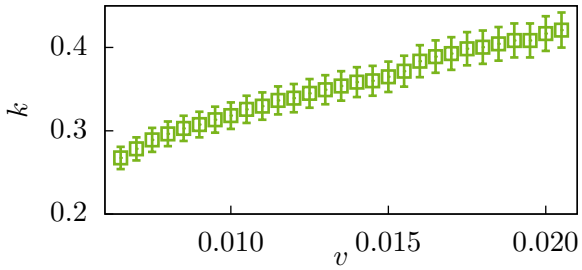

Figure 5.3.: Wavenumber of the stripe pattern vs. the transfer velocity v as obtained from 2D direct numerical simulations of equations (5.1) with $\alpha = 2.3$.

5.3.2. Transition to Hexagonal Patterns

Especially for small initial concentrations, the spinodal instability occurring in the region of the contact line preferably leads to the formation of aligned droplets, rather than stripes. This can be seen in analogy to the dynamics shown for the classical Cahn-Hilliard equation in figure 3.2, where for small initial concentration, the formation of droplets is preferred over the formation of labyrinth-like patterns. Due to the same mechanism as described in the previous subsection, the structures of aligned droplets recur periodically. In subsequent lines, the droplets are arranged shifted to each other, such that a pattern of hexagonal type is transferred onto the substrate (see figure 5.5).
In our simulations, in general the hexagonal patterns occur subsequent to a transient regime of stripe patterns and for various initial concentrations. The stripe patterns become unstable through a transversal instability. It is unclear and to be verified by an appropriate stability analysis, if all regimes of stripe pattern formation are unstable to an instability leading to hexagonal patterns. As for the stripes, coarsening dynamics of the transferred hexagones can be observed, leading to defects which are advected away from the contact line and do not influence the overall regime of pattern formation.

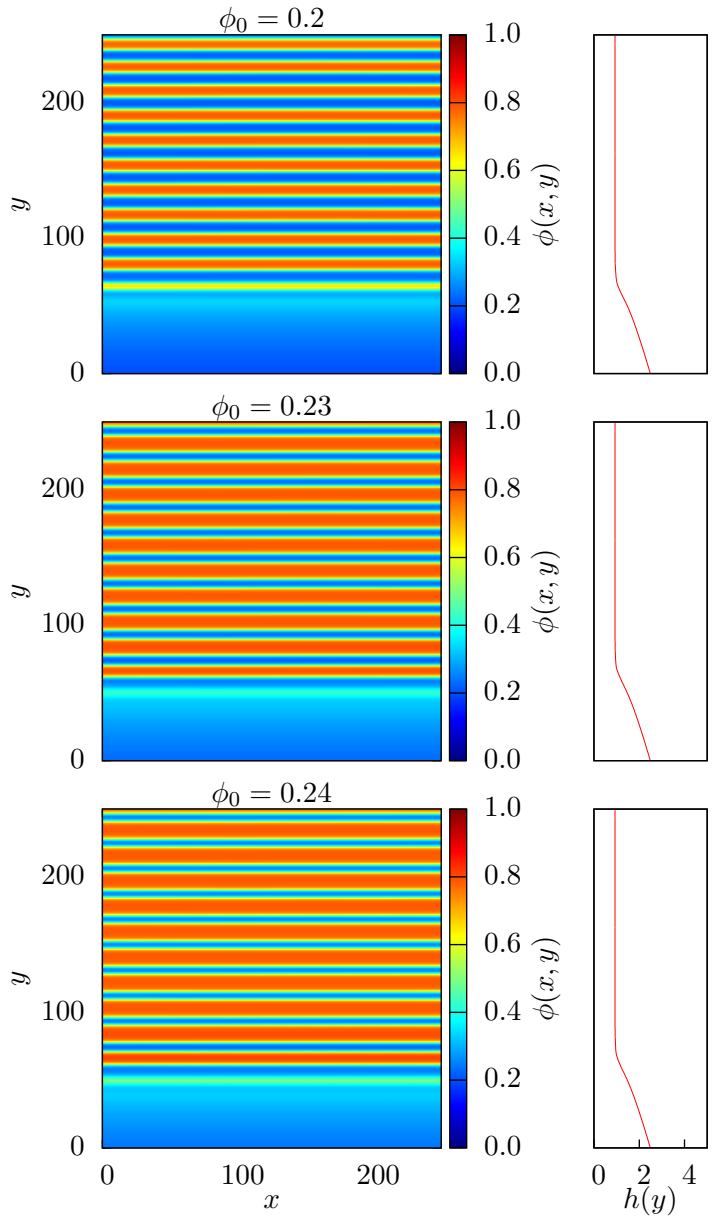

Figure 5.4.: Snapshots of 2D simulations of the full equations (5.1), for $\alpha = 2.3$ and three different initial concentrations ϕ_0. The width of the stripes formed at the meniscus increases with the initial concentration ϕ_0. On the right, the corresponding meniscus shape is shown as a cross-section at $x = L/2$.

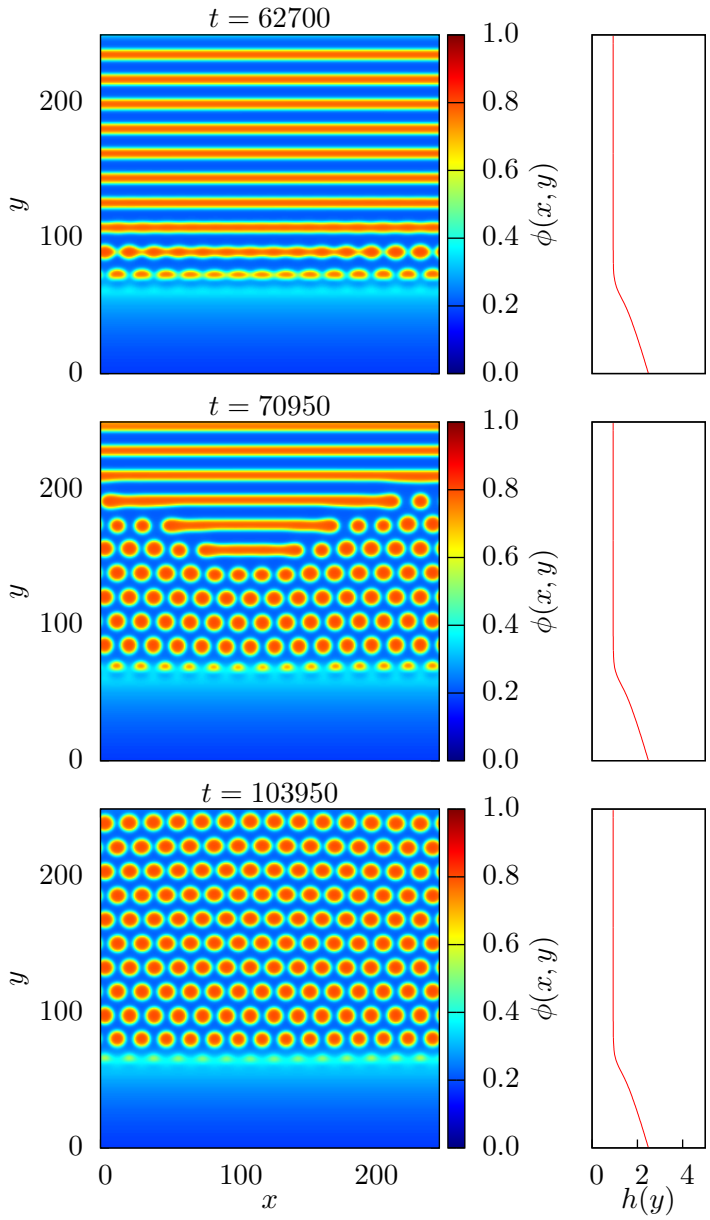

Figure 5.5.: Snapshots of 2D simulations of the model equations (5.1) showing the transition from a stripe pattern to a hexagonal pattern. The instability is initiated by transversal instabilities of the stripes in proximity to the meniscus. The initial concentration is $\phi_0 = 0.18$.

5.3.3. Comparison to Similar Models

In the previous part of this chapter, we have shown that through a very complicated process of directional phase decomposition periodic structures were formed. It is similar to the process of pattern formation as it is described for a full model [LKG$^+$12] and a simplified model [KGFT12] for the case of the Langmuir-Blodgett transfer. An even more simple model showing directional phase separation in the Cahn-Hilliard equation is investigated in [Kre09]. There, the classical Cahn-Hilliard equation with the free energy density

$$f(c) = \frac{1}{4}c^4 - \frac{\epsilon(x,t)}{2}c^2, \quad \text{where} \quad \epsilon = \begin{cases} -\epsilon & \text{if } x < y(t) \\ +\epsilon & \text{if } \epsilon > y(t) \end{cases} \tag{5.6}$$

is subjected to a front which is localized at $y(t)$, moves with a constant velocity v and switches the sign of ϵ, thus inducing a linear instability at the front position. In this system, periodic stripe patterns are observed for a straight front in one and two dimensions. For a sinusoidally modulated front, vertically oriented stripes and hexagonal patterns are found, depending on the transfer speed. For this simple model, an analytical treatment was possible in terms of a *marginal stability analysis*. In our system, analogous calculations are rather difficult, since they necessitate knowledge about the concentration influx at the region where the pattern formation sets in. A project for future work could be to implement boundary conditions which control the flux at $y = 0$. It should be discussed if such boundary conditions are physically more meaningful than the ones employed in the current model.
To summarize, the comparison of our results with [LKG$^+$12, KGFT12, Kre09] shows that in our rather complicated process of phase decomposition, we obtain structures which seem archetypical for directed phase decomposition.

6. Summary and Outlook

As stated in the introductory chapter, this work represents a first step towards a hydrodynamic model for thin solution layers, which has the ability to describe the deposition of complex structures in dip-coating experiments. We will now summarize the content of the thesis and give an outlook for future work.
In chapter 2, we presented a derivation of thin film equations for dilute solutions through the application of a long-wave expansion to advection-diffusion equations. The derived equations account for an evaporative contribution, the advection of the substrate and a concentration-dependent viscosity of the fluid.
Referring to [Thi11], we showed in chapter 3 that the conservative part of our basic equations can be written in terms of a gradient formulation. We then presented an extension of the equations, where the bulk free energy was chosen according to the free energy of a regular solution. The extension leads to contributions of concentration gradients in the advective flux and an alternated diffusional flux, which now allows for phase separation in the concentration field, i.e., solvent-solute demixing. In analogy to the derivation presented in chapter 2, we proposed a derivation for the general form of the extended diffusional dynamics.
In the following chapter, we discussed a particular choice of the evaporation term, which is concentration-dependent through contributions of osmotic type. We showed that due to the entropic contribution in the solvent concentration, the evaporation is always saturated for solute concentrations lower than unity. This is an improvement over models used in literature where the evaporation is concentration independent. Nevertheless, we were only able to treat the evaporation term numerically for particular choices of the parameters involved. Here, a concentration-dependent disjoining pressure could lead to better results, which however is at the expense of the simplicity of the model. We then investigated the linear stability of the full equations as well as the dynamics of phase separation and dewetting. The linear stability analysis revealed that the coupling of the concentration to the height of the film is of simple nature in our model. However, the nonlinear coupling of concentration gradients to the advective flux was shown to lead to interesting effects.
Finally, in chapter 5, we presented first results concerning the formation of periodic structures in dip-coating experiments. In the simulations, the local solute height is always smaller than unity, in this case the evaporation term leads to an approximately constant film height of the transferred layer, independent of the concentration. In the simulations presented in chapter 5, stripe patterns parallel to the contact line, as well as patterns of hexagonal type, are formed due to evaporation-induced phase decomposition.

The structures shown in this chapter were also found in similar models describing directed phase decomposition based on a Cahn-Hilliard approach. In the literature, the formation of stripe patterns at the receding contact line of evaporating solutions and suspension is reported, e.g., for polymer solutions [HXL07] or colloidal suspensions [BDG10]. In contrast to our model, the formation is explained by a stick-slip motion of the contact line in these experiments.

As it should be the case for a first approach, the present thesis opens many perspectives for future work. The conservative part of our equations consists of coupled PDEs describing dewetting as well as phase separation in a non-conserved order parameter. It would be interesting to investigate the coupling of the two processes in more detail for a simplified bulk free energy. Here, especially the coupled coarsening dynamics would be of interest.
While our formulation of the evaporation term is certainly a step into the right direction, it still needs to be improved, e.g., as proposed above through the formulation of a concentration-dependent disjoining pressure.
In order to describe the formation of structures at a receding contact-line, two strategies, can be pursued. On the one hand, our current model can be used to investigate the deposition of solute-structures for larger local values of Ψ, leading to a concentration-dependent height in the transferred layer. This would necessitate the consideration of larger initial film heights, which is numerically difficult to treat for the disjoining potential (4.3) currently used. Since evaporation is included in our model, a possible ansatz could be to consider a completely wetting liquid with a disjoining potential which is simply of van der Waals type. In this case, the numerical treatment of larger film heights would be simpler. Although the current model might seem quite extensive, some physical effects which could be important for the formation of complex structures are still neglected. For example, the surface tension of the film should not be independent of large concentrations. Furthermore, the bulk free energy currently used is still of a very simplifying nature. For the description of the structures reported in [LGS$^+$10], it seems probable that a bulk free energy accounting for anisotropic particles is necessary. Nevertheless, all extensions of the model should be well reflected, in order to preserve the possibilities to treat the model numerically or even partially analytically, which is quite difficult even for the current model.
For this reason, the second strategy which could be pursued is the formulation of a more simple and abstract model of phase-field type [WB95] for the formation of deposition structures. The process of deposition is a solidification process after all, and such processes are successfully described by phase-field models, e.g., for the case of metals. Nevertheless, this ansatz could not account for hydrodynamic effects on the formation of the structures and should only be pursued in addition to a further development of our current model.

A. Appendix

In this appendix, we give a short overview of the numerical methods employed for the simulations shown in the thesis. The program used is written based on a solver developed by Markus Wilczek in the context of his Master thesis [Wil12].

A.1. Finite Differences

The spatial partial derivatives occurring in the treated equations are evaluated in terms of *central finite differences*. This method is a straight-forward discretisation of the derivatives based on their mathematical definition as the limit of difference quotients. We will explain the basic idea for the case of a first order derivative and then give an overview of the higher order finite differences used, referring the interested reader to [Bes06] for more details.
To obtain the first order derivative of a function $f(x)$ with respect to a discretisation Δx and with a second order accuracy, we perform the following Taylor expansion:

$$\begin{aligned} f(x+\Delta x) - f(x-\Delta x) &= f(x) + f'(x)\Delta x + \mathcal{O}(\Delta x^2) - f(x) + f'(x)\Delta x + \mathcal{O}((\Delta x)^2) \\ &= f'(x)(2\Delta x) + \mathcal{O}(x^2). \end{aligned}$$

Using the notation $f(x) =: f_i$, $f(x \pm \Delta x) =: f_{i\pm1}$, we obtain the central difference representation of a first order derivative as

$$f_i' = \frac{f_{i+1} - f_{i-1}}{2\Delta x}. \tag{A.1}$$

The extension to the case of partial derivatives of a function $f(x,y) =: f_{ij}$ is straightforward. In this thesis, the following discretised differential operators were employed:

$$\partial_x f_{ij} = \frac{f_{i+1,j} - f_{i-1,j}}{2\Delta x}; \quad \partial_y f(x,y) = \frac{f_{i,j+1} - f_{i,j-1}}{2\Delta x}; \tag{A.2}$$

$$\Delta f_{ij} = \frac{f_{i+1,j} + f_{i-1,j} + f_{i,j+1} + f_{i,j-1} - 4f_{i,j}}{(\Delta x)^2} \tag{A.3}$$

For the simulations shown in this thesis, we used discretisations with a number of grid points in x, and y direction ranging from $N_{x,y} = 170$ to $N_{x,y} = 400$, according to the respective domain size.

A.2. Boundary Conditions

For the numerical treatment, our basic equations were written in terms of the variables ρ and Ψ. As for the formulation in h, Ψ, in these variables the conservative part of our equations takes the form of a continuity equation (3.28). In order to obtain numerical solutions which respect the corresponding conservation constraints, the finite differences had to be applied first to obtain the flux field, and then, successively to calculate the divergence of the flux. This successive treatment in terms of finite differences necessitates the definition of three virtual grid points and of three corresponding boundary conditions at each boundary.
For the simulations of the transfer process shown in chapter 5, the upper and lower boundary conditions can be expressed in terms of the finite differences. This yields expressions for the virtual grid points $f_{i,-1}, f_{i,-2}, f_{i,-3}$ and $f_{i,Ny}, f_{i,Ny+1}, f_{i,Ny+2}$ in terms of neighboring grid points corresponding to the physical simulation domain. For the case of the boundary conditions (5.3), we obtain through simple calculations:

$$f_{i,-1} = f_0; \quad f_{i,-2} = 2f_0 - f_{i,0}; \quad f_{i,-3} = 4f_0 - 4f_{i,0} + f_{i,1}, \tag{A.4}$$

$$f_{i,N_x+2} = f_{i,N_x+1} = f_{i,N_x} = f_{i,N_x-1}. \tag{A.5}$$

Note that the boundary conditions are located at the first virtual grid point, rather than at the last physical one.

A.3. CUDA Framework

In the framework of calculations based on finite differences, at each grid point only neighboring grid points are of relevance. Especially for the case of two dimensional calculations, the use of parallelised algorithm is therefore useful and possible. In our case, the parallelised calculations are performed using modern GPUs (Graphics Processing Units). These GPUs are predestined for parallelised calculations, since they are constituted of a few thousand processing cores. Note that the single cores of the GPUs are much slower than an ordinary CPU and the speed-up through the use of GPUs is only achieved due to the large number of parallel calculations. GPUs are accessible for general purpose calculations, e.g., through the so called CUDA framework, which is based on C++.
The internal parallelisation of the calculations on the GPU is organized in terms of so-called *Blocks* of *Threads* . More precisely, the grid resulting from the spacial discretisation is divided into Blocks containing a certain number of grid points, where each grid point is treated by one Thread. The data corresponding to one Block is stored in a shared memory, allowing a fast access on the data necessary for the calculations within the Block. In each timestep, the calculations in the Blocks are performed parallelised. Therefore, each Block also comprehends virtual grid points, corresponding to the actual calculation domain of neighboring Blocks. In summary, our calculations in terms of finite differences are well adapted to this framework of parallelised calculations, which

leads to a considerable speed-up of the numerical treatment. For further information about the CUDA framework, the reader is referred to [NVI].

A.4. Time-Stepping

In order to solve the large system of coupled ODEs resulting from the spatial discretisation, we use an explicit Runge-Kutta Dormand-Prince algorithm with an adaptive step-size. Runge-Kutta time-stepping algorithms are extensions of the classical Euler-Forward algorithm with higher order accuracy. The general form of a Runge-Kutta algorithm for an ODE

$$\partial_t x = F(x(t), t) \tag{A.6}$$

is of the type

$$x(t + \Delta t) = x(t) + \Delta t \sum_{i=1}^{n} \gamma_i k_i, \tag{A.7}$$

$$\text{where} \quad k_i = F(x(t) + \Delta t \sum_{j=1}^{i-1} \beta_{ij} k_j, t + \alpha_i \Delta t). \tag{A.8}$$

Here, n determines the stage of the method, while the order of accuracy does not necessarily correspond to the stage n. The coefficients vary according to the specific Runge-Kutta scheme considered. In general, the coefficients are organized in so called *Butcher-Tableaus* specifying a method. In adaptive algorithms, the time stepping is performed with two Runge-Kutta schemes of different orders of accuracy. A comparison of both algorithms is used for an estimation of the numerical error ϵ being made in each time-step. According to the numerical error, the time step-size Δt is adjusted in order to ensure the error to stay below a given threshold. For details about the Runge-Kutta Dormand-Prince algorithm and its explicit form, the reader is referred to [But08].

Bibliography

[AC79] S.M. Allen and J.W. Cahn. A microscopic theory for antiphase boundary motion and its application to antiphase domain coarsening. *Acta Metallurgica*, 27(6):1085–1095, 1979.

[BDG10] H. Bodiguel, F. Doumenc, and B. Guerrier. Stick-slip patterning at low capillary numbers for an evaporating colloidal suspension. *Langmuir*, 26(13):10758–10763, 2010.

[Bes06] M. Bestehorn. *Hydrodynamik und Strukturbildung: Mit einer kurzen Einführung in die Kontinuumsmechanik*. Springer, 2006.

[BMW02] G.K. Batchelor, H.K. Moffatt, and M.G. Worster. *Perspectives in fluid dynamics: a collective introduction to current research*. Cambridge University Press, 2002.

[But08] J.C. Butcher. *Numerical methods for ordinary differential equations*. John Wiley & Sons, 2008.

[CH58] J.W. Cahn and J.E. Hilliard. Free energy of a nonuniform system. i. interfacial free energy. *The Journal of Chemical Physics*, 28:258, 1958.

[CH59] J.W. Cahn and J.E. Hilliard. Free energy of a nonuniform system. iii. nucleation in a two-component incompressible fluid. *The Journal of Chemical Physics*, 31:688, 1959.

[Cla04] N. Clarke. Instabilities in thin-film binary mixtures. *The European Physical Journal E*, 14(3):207–210, 2004.

[CM09] R.V. Craster and O.K. Matar. Dynamics and stability of thin liquid films. *Reviews Of Modern Physics*, 81(3):1131, 2009.

[CWS+02] M.L. Chabinyc, W.S. Wong, A. Salleo, K.E. Paul, and R.A. Street. Organic polymeric thin-film transistors fabricated by selective dewetting. *Applied Physics Letters*, 81(22):4260–4262, 2002.

[deG79] P.-G. deGennes. *Scaling concepts in polymer physics*. Cornell University Press, 1979.

[Der40] B. Derjaguin. *Zh. Fiz. Khim.*, 14:137, 1940.

[Ein06] A. Einstein. Zur Theorie der Brownschen Bewegung. *Annalen der Physik*, 324(2):371–381, 1906.

[FAT11] L. Frastia, A.J. Archer, and U. Thiele. Dynamical model for the formation of patterned deposits at receding contact lines. *Physical Review Letters*, 106(7):077801, 2011.

[FAT12] L. Frastia, A.J. Archer, and U. Thiele. Modelling the formation of structured deposits at receding contact lines of evaporating solutions and suspensions. *Soft Matter*, 8(44):11363–11386, 2012.

[GFS07] M. Ghosh, F. Fan, and K.J. Stebe. Spontaneous pattern formation by dip coating of colloidal suspensions on homogeneous surfaces. *Langmuir*, 23(4):2180–2183, 2007.

[God91] C. Godrèche. *Solids far from Equilibrium*, volume 1. Cambridge University Press, 1991.

[GP71] P. Glansdorff and I. Prigogine. *Thermodynamic theory of structure, stability and fluctuations*. Cambridge University Press, 1971.

[GR93] W. Greiner and J. Reinhardt. *Feldquantisierung*, volume 7. 1993.

[Gug35] E.A. Guggenheim. The statistical mechanics of regular solutions. *Proceedings of the Royal Society of London. Series A-Mathematical and Physical Sciences*, 148(864):304–312, 1935.

[Hil60] T.L. Hill. *An introduction to statistical thermodynamics*. Dover Publications, 1960.

[HS71] C. Huh and L.E. Scriven. Hydrodynamic model of steady movement of a solid/liquid/fluid contact line. *Journal of Colloid and Interface Science*, 35(1):85–101, 1971.

[HW91] H. Haken and A. Wunderlin. *Die Selbststrukturierung der Materie*. Vieweg, 1991.

[HXL07] S.W. Hong, J. Xia, and Z. Lin. Spontaneous formation of mesoscale polymer patterns in an evaporating bound solution. *Advanced Materials*, 19(10):1413–1417, 2007.

[HXX+05] S.W. Hong, J. Xu, J. Xia, Z. Lin, F. Qiu, and Y. Yang. Drying mediated pattern formation in a capillary-held organometallic polymer solution. *Chemistry of Materials*, 17(25):6223–6226, 2005.

[Isr11] J.N. Israelachvili. *Intermolecular and surface forces: revised third edition*. Academic press, 2011.

[KGFC10] M.H. Köpf, S.V. Gurevich, R. Friedrich, and L. Chi. Pattern formation in monolayer transfer systems with substrate-mediated condensation. *Langmuir*, 26(13):10444–10447, 2010.

[KGFT12] M.H. Köpf, S.V. Gurevich, R. Friedrich, and U. Thiele. Substrate-mediated pattern formation in monolayer transfer: a reduced model. *New Journal of Physics*, 14(2):023016, 2012.

[Köp11] M.H. Köpf. *On the Dynamics of Surfactant Covered Thin Liquid Films and the Formation of Stripe Patterns in Langmuir-Blodgett Transfer*. PhD thesis, Münster University, 2011.

[Kre09] A. Krekhov. Formation of regular structures in the process of phase separation. *Physical Review E*, 79(3):035302, 2009.

[KT07] S. Kalliadasis and U. Thiele. *Thin Films of Soft Matter*, volume 490. Springer, 2007.

[LG05] Z. Lin and S. Granick. Patterns formed by droplet evaporation from a restricted geometry. *Journal of the American Chemical Society*, 127(9):2816–2817, 2005.

[LGP02] A.V. Lyushnin, A.A. Golovin, and L.M. Pismen. Fingering instability of thin evaporating liquid films. *Physical Review E*, 65(2):021602, 2002.

[LGS+10] L. Li, P. Gao, K.C. Schuermann, S. Ostendorp, W. Wang, C. Du, Y. Lei, H. Fuchs, and L.D. et al. Cola. Controllable growth and field-effect property of monolayer to multilayer microstripes of an organic semiconductor. *Journal of the American Chemical Society*, 132(26):8807–8809, 2010.

[LKG+12] L. Li, M.H. Köpf, S.V. Gurevich, R. Friedrich, and L. Chi. Structure formation by dynamic self-assembly. *Small*, 8(4):488–503, 2012.

[LL70] L.D. Landau and E.M. Lifšic. *Statistische Physik*. Lehrbuch der theoretischen Physik. Akademie-Verlag, 1970.

[LLW91] L.D. Landau, E.M. Lifšic, and W. Weller. *Hydrodynamik*. Lehrbuch der theoretischen Physik. Akademie-Verlag, 1991.

[LT98] J. Lowengrub and L. Truskinovsky. Quasi–incompressible cahn–hilliard fluids and topological transitions. *Proceedings of the Royal Society of London. Series A: Mathematical, Physical and Engineering Sciences*, 454(1978):2617–2654, 1998.

[NCS84] A. Novick-Cohen and L.A. Segel. Nonlinear aspects of the Cahn-Hilliard equation. *Physica D: Nonlinear Phenomena*, 10(3):277–298, 1984.

[NT10] L. Náraigh and J.-L. Thiffeault. Nonlinear dynamics of phase separation in thin films. *Nonlinearity*, 23(7):1559, 2010.

[NVI] NVIDIA. CUDA C Programming Guide Version 4.2. `http://docs.nvidia.com/cuda/cuda-c-programming-guide/index.html`. last visited on December 1st, 2013.

[ODB97] A. Oron, S.H. Davis, and S.G. Bankoff. Long-scale evolution of thin liquid films. *Reviews of Modern Physics*, 69(3):931, 1997.

[PBMT05] A. Pototsky, M. Bestehorn, D. Merkt, and U. Thiele. Morphology changes in the evolution of liquid two-layer films. *The Journal of Chemical Physics*, 122(22):224711–224711, 2005.

[Pis01] L.M. Pismen. Nonlocal diffuse interface theory of thin films and the moving contact line. *Physical Review E*, 64(2):021603, 2001.

[Pis06] L.M. Pismen. *Patterns and interfaces in dissipative dynamics*. Springer, 2006.

[Pro05] R.F. Probstein. *Physicochemical hydrodynamics: an introduction*. Wiley, 2005.

[Que77] D. Quemada. Rheology of concentrated disperse systems and minimum energy dissipation principle. *Rheologica Acta*, 16(1):82–94, 1977.

[Rei92] G. Reiter. Dewetting of thin polymer films. *Physical Review Letters*, 68:75–78, 1992.

[Saf94] S.A. Safran. *Statistical thermodynamics of surfaces, interfaces, and membranes*. Addison-Wesley Reading, 1994.

[Sha93] A. Sharma. Relationship of thin film stability and morphology to macroscopic parameters of wetting in the apolar and polar systems. *Langmuir*, 9(3):861–869, 1993.

[Thi11] U. Thiele. Note on thin film equations for solutions and suspensions. *The European Physical Journal Special Topics*, 197(1):213–220, 2011.

[Thi14] U. Thiele. Patterned deposition at moving contact lines. *Advances in Colloid and Interface Science doi:10.1016/j.cis.2013.11.002;*, 2014.

[Tod13] D.V. Todorova. *Modelling of dynamical effects related to the wettability and capillarity of simple and complex liquids*. PhD thesis, Loughborough University, 2013.

[TTL13] U. Thiele, D.V. Todorova, and H. Lopez. Gradient dynamics description for films of mixtures and suspensions: Dewetting triggered by coupled film height and concentration fluctuations. *Physical Review Letters*, 111(11):117801, 2013.

[TVA+09] U. Thiele, I. Vancea, A.J. Archer, M.J. Robbins, L. Frastia, A. Stannard, E. Pauliac-Vaujour, C.P. Martin, M.O. Blunt, and P.J. Moriarty. Modelling approaches to the dewetting of evaporating thin films of nanoparticle suspensions. *Journal of Physics: Condensed Matter*, 21(26):264016, 2009.

[WB95] J.A. Warren and W.J. Boettinger. Prediction of dendritic growth and microsegregation patterns in a binary alloy using the phase-field method. *Acta Metallurgica et Materialia*, 43(2):689–703, 1995.

[WCM03] M.R.E. Warner, R.V. Craster, and O.K. Matar. Surface patterning via evaporation of ultrathin films containing nanoparticles. *Journal of Colloid and Interface Science*, 267(1):92–110, 2003.

[Wil12] M. Wilczek. Pattern formation in Cahn-Hilliard models for Langmuir-Blodgett transfer, Master thesis, Münster University, 2012.

Danksagung

Zum Ende dieser Masterarbeit möchte ich folgenden Personen meinen Dank aussprechen:

- Herrn Prof. Dr. Andreas Heuer, für die zuvorkommende Bereitschaft die Betreuung und Begutachtung dieser Arbeit zu übernehmen.
- Frau Dr. Svetlana Gurevich, für eine sehr freundliche und engagierte Betreuung, sowie das große Vertrauen.
- Herrn Prof. Dr. Uwe Thiele, für seine fachliche Unterstützung mit richtungsweisenden Ratschlägen.
- Herrn Markus Wilczek, für seine großartige Hilfsbereitsschaft und Unterstützung während des gesamten Verlaufs der Arbeit, sowie für das Korrekturlesen dieser Arbeit.
- Meinen Büro-Kollegen Alexander Kraft und Felix Tabbert für eine schöne Atmosphäre im Büro, sowie Felix Tabbert ebenfalls für das Korrekturlesen der Arbeit.
- Der gesamten Arbeitsgruppe für schöne Mittagspausen und Hilfestellung in vielen Details.
- Meinen Eltern, sowie meiner Schwester Ida, für ihre bedingungslose Unterstützung während meines gesamten Studiums.

Erklärung zur Masterarbeit

Hiermit versichere ich, die vorliegende Masterarbeit selbstständig angefertigt und außer den angegebenen keine weiteren Hilfsmittel und Quellen verwendet zu haben. Zitate habe ich kenntlich gemacht.

Münster, den 05. Dezember 2013